Available online at www.sciencedirect.com
ScienceDirect
Journal of Sound and Vibration 298 (2006) 108–131
JOURNAL OF SOUND AND VIBRATION
www.elsevier.com/locate/jsvi

Elastic wave radiation from a high frequency finite-length transducer

G.W. Owen[a,*], I.D. Abrahams[b]

[a]Department of Mathematics, Keele University, Keele, Staffordshire, UK
[b]Department of Mathematics, University of Manchester, Oxford Road, Manchester, UK

Received 11 July 2005; received in revised form 27 March 2006; accepted 24 April 2006
Available online 7 July 2006

Abstract

A simple model of a high frequency piezoelectric transducer affixed to an elastic half-space is analysed. The problem is reformulated as a modified matrix Wiener–Hopf equation, containing a kernel for which there is no known exact factorisation. An approximate factorisation is obtained, and the resulting integral equation is solved by iteration, in limit that the length of the transducer is very much larger than a typical wavelength.

1. Introduction

Problems concerning the propagation, refraction and diffraction of waves are the subject of a great deal of work by both theoretical and experimental scientists. The detection of cracks and other defects in solid bodies is of vital importance in a wide variety of practical applications, such as ensuring reliability of components in engines and gearboxes. In the field of non-destructive testing, one method to detect defects is to analyse the scattering of the elastic waves generated by ultrasonic transducers. To gain understanding of the way in which transducers (placed on a free surface of an elastic specimen) generate the elastic waves used to insonify the defect, it is important to study in detail some simple models.

A property which differentiates the theory of elastic waves from acoustic and water waves is that elastic bodies support two distinct types of body waves, which are either compressional (longitudinal) or shear (transverse) in nature. These wave fields are typically coupled at the boundary or interface of an elastic body; a wave of one type which is incident upon such a interface will undergo mode conversion and the resulting reflected wave will be composed of both wave types. Furthermore, such interfaces may support surface waves such as the Rayleigh wave.

A full mathematical model of the interactions between an elastic body and such a piezoelectric transducer, such as that used by Rogers [1], requires consideration of a large number of parameters. In addition to the properties of the body under examination, it would be necessary to model the elasticity of the transducer and its electroelastic coupling with the driving electromagnetic force. Such a model is too difficult to investigate

*Corresponding author. Tel.: +44 1782 583780; fax: +44 1782 584268.
E-mail address: g.w.owen@maths.keele.ac.uk (G.W. Owen).

0022-460X/$ - see front matter © 2006 Elsevier Ltd. All rights reserved.
doi:10.1016/j.jsv.2006.04.039

using the analytical techniques of diffraction theory. However, if we are interested only in the wave field induced by a transducer in the body under test, or the diffracting properties of a model defect, we may make simplifying assumptions about the physical properties of the transducer/defect, and assuming the specimen to be of infinite extent we may make progress toward finding the resulting acoustic wave field. Such an approach has proved fruitful, and progress has been made in determining the wavefield using both analytic and numerical techniques. We now briefly mention several key works looking at these basic models.

Lapwood [2] showed analytically that a general solution for elastic waves in a half-space could be expressed in terms of Green's functions for a pair of coupled Helmholtz equations, representing the solutions for a line source of compressional and shear waves. These Green's function solutions have been widely utilised. Wickham [3,4] applied them to analyse a model transducer performing prescribed oscillations in the y-direction, but lubricated such that the tangential stresses vanish across the entire surface. This approximation was made purely for mathematical convenience, in order to obtain a tractable, scalar, integral equation representation for the unknown normal stresses under the transducer. This problem was solved by iteration in the high-frequency limit, with results showing good agreement with the Geometrical Theory of Diffraction, as discussed by Achenbach et al. [5].

Within the context of soil/structure interaction, Flitman [6] studied the interaction between a seismic wave and a rigid strip in smooth contact with the surface of an elastic half-space (i.e. the same simplified boundary conditions as that used in Refs. [3,4]), and used the Wiener–Hopf technique to obtain a transient description of the stress exerted on the base of the strip. Oien [7] extended that work to a strip in fully bonded contact (as in this work), approximately solving a pair of coupled Fredholm integral equations using the Galerkin method to obtain the equivalent influence functions.

The formulation of elastodynamical problems as integral equations has also led to novel numerical method for their solution. In particular, the boundary element method [8] allows the problem's dimensionality to be reduced and numerical solutions to be found. However, as with other direct numerical schemes, such as finite differences, the singular field near the transducer edges cannot be modelled accurately. An in-depth review of the application of these methods may be found in Beskos [9]. More recently, the semi-numerical asymptotic approach of Gridin and Fradkin [10], which captures the edge behaviour correctly, has allowed progress to be made in evaluating the wavefield induced by a circular transducer in three dimensions.

This article offers an analytical (but approximate) technique to evaluate the elastic wave field generated by a finite, planar transducer, and details are given for the simplest case of a rigid transducer. In our model the transducer will be represented by a prescribed displacement field over a region of the surface of width much greater than a typical body wavelength. The approach employed herein is the modified Wiener–Hopf technique (see Noble [11]). We shall formulate this model as a three-part mixed boundary value problem for the compressional and shear wave potentials. The coupling between these potentials means, after the application of a suitable Fourier transform, that the resulting modified Wiener–Hopf equation has a complicated matrix kernel. There is no known procedure for factorising this matrix kernel exactly into factors with the properties necessary for the application of the Wiener–Hopf technique. However, Abrahams' [12,13] method of obtaining an approximate factorisation may be applied and appears to give very accurate results at little numerical cost. This procedure, and the symmetry of the problem enables us to form a vector integral equation, which in the high frequency limit, may be solved approximately by iteration. We thus obtain the first two non-zero terms of a perturbation expansion, as well as offering a procedure for determining higher order terms.

The paper is arranged as follows. In the next section the boundary value problem is specified in terms of two elastic potentials. Fourier transforms are introduced in Section 3 and by their application the problem is reduced to a modified matrix Wiener–Hopf equation, valid in a specified strip of the complex plane. The solution of this equation relies on the successful factorization of the Wiener–Hopf kernel, which is accomplished approximately in Section 4, as well as an asymptotic decomposition of two vector integral equations described in Section 5. The latter relies on the transducer being long in comparison to the elastic wavelengths. Simple forcing is studied in the preliminary sections, but the solution for arbitrary loading on the finite strip is discussed in Section 6. Numerical solutions are offered in Section 7, together with an energy balance calculation to indicate the accuracy of the present approach. Final remarks and suggestions for further work are made in the concluding section of the paper.

2. The boundary value problem

We model the body under inspection as a homogeneous, isotropic, elastic half-space occupying the region $y \geqslant 0$, $-\infty < x, z < \infty$, where (x, y, z) are Cartesian coordinates. The induced displacement field $\mathbf{u} = (u, v, w)$ (acting in the (x, y, z) directions) can be shown (see Gould [14], for example) to satisfy Navier's equation:

$$\mu \nabla^2 \mathbf{u} + (\lambda + \mu) \operatorname{grad} \operatorname{div} \mathbf{u} = \rho \frac{\partial^2}{\partial t^2} \mathbf{u}, \tag{1}$$

where ρ is the density, λ, μ the Lamé constants of the material and t is the time. The half-space is forced by a transducer of length $2l$ which, for mathematical convenience, is represented by a perfectly rigid, finite width, strip placed in contact with the surface of the half-space, as shown in Fig. 1. The transducer occupies the region $y = 0$, $-l < x < l$, and performs prescribed in-plane harmonic motion, with angular frequency ω. Thus, for $|x| < l$, $y = 0$ we have

$$u = u_0(x) \mathrm{e}^{-\mathrm{i}\omega t}, \quad v = v_0(x) \mathrm{e}^{-\mathrm{i}\omega t}, \quad w = 0. \tag{2}$$

The remainder of the surface is free, i.e. the normal and tangential stresses are identically zero. Denoting the elements of the stress tensor as σ_{ij}, we have, for $y = 0$, $|x| > l$,

$$\sigma_{12} = \mu \left(\frac{\partial u}{\partial y} + \frac{\partial v}{\partial x} \right) = 0, \quad \sigma_{22} = \lambda \boldsymbol{\nabla} \cdot \mathbf{u} + 2\mu \frac{\partial v}{\partial y} = 0. \tag{3}$$

Since the forcing is in-plane, the entire displacement field is in-plane (i.e. $w \equiv 0$). Hence, for time-harmonic motion, the displacement field may be expressed in terms of complex-valued compressional and shear potential functions, $\phi(x, y)$ and $\psi(x, y)$, in the form

$$\mathbf{u} = \operatorname{Re}\{\hat{\mathbf{u}} \mathrm{e}^{-\mathrm{i}\omega t}\} = \operatorname{Re}\{[\operatorname{grad} \phi + \operatorname{curl}(\psi \mathbf{e}_z)] \mathrm{e}^{-\mathrm{i}\omega t}\}, \tag{4}$$

where $\mathbf{e}_z$ is the unit vector in the z direction. Substitution of Eq. (4) into Eq. (1), results in a pair of Helmholtz equations

$$\nabla^2 \phi + k^2 \phi = 0, \tag{5}$$

$$\nabla^2 \psi + K^2 \psi = 0, \tag{6}$$

where the wavenumbers k and K are given by

$$k^2 = \frac{\rho \omega^2}{\lambda + 2\mu} \quad \text{and} \quad K^2 = \frac{\rho \omega^2}{\mu}. \tag{7}$$

Eqs. (5) and (6) are coupled at the boundary $y = 0$ such that the boundary conditions (Eqs. (2) and (3)) become

$$\frac{\partial \phi}{\partial x} + \frac{\partial \psi}{\partial y} = u_0(x), \qquad \frac{\partial \phi}{\partial y} - \frac{\partial \psi}{\partial x} = v_0(x), \quad |x| < l, \tag{8}$$

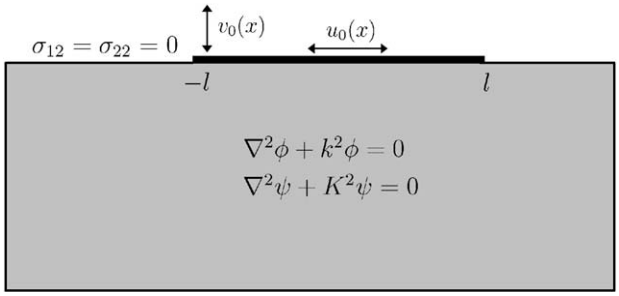

Fig. 1. The elastic half-space with stress free and imposed displacement boundary conditions.

$$2\frac{\partial^2\phi}{\partial x\partial y}+\frac{\partial^2\psi}{\partial y^2}-\frac{\partial^2\psi}{\partial x^2}=0, \quad |x|>l, \tag{9}$$

$$\frac{K^2}{k^2}\left\{\frac{\partial^2\phi}{\partial x^2}+\frac{\partial^2\phi}{\partial y^2}\right\}-2\frac{\partial^2\phi}{\partial x^2}-2\frac{\partial^2\psi}{\partial x\partial y}=0, \quad |x|>l. \tag{10}$$

To guarantee a unique solution it is necessary to impose two further conditions. Firstly, we impose the Sommerfeld radiation condition requiring that the radiated wave-field is outgoing in nature. Secondly, we require that the displacements everywhere, (and in particular at $x=\pm l$, $y=0$) remain finite. This boundary value problem is to be solved approximately using the modified Wiener–Hopf technique, first utilised by Jones [15].

3. Reduction to a modified matrix Wiener–Hopf equation

The boundary value problem may be reduced to a modified matrix Wiener–Hopf equation by expressing the potentials in terms of Fourier integrals of the form

$$\phi(x,y)=\frac{1}{2\pi}\int_{\mathscr{C}}\Phi(\alpha,y)\mathrm{e}^{-\mathrm{i}\alpha x}\,\mathrm{d}\alpha, \tag{11}$$

$$\psi(x,y)=\frac{1}{2\pi}\int_{\mathscr{C}}\Psi(\alpha,y)\mathrm{e}^{-\mathrm{i}\alpha x}\,\mathrm{d}\alpha, \tag{12}$$

where the contour $\mathscr{C}$ is chosen as shown in Fig. 2, i.e. indented well away from the points $\pm k$, $\pm K$, for reasons to be made clear in due course.

Using the well known inversion formulae for the Fourier transforms defined in Eqs. (11) and (12) and exchanging the order of integration and differentiation, the equations of motion (5) and (6) may be rewritten in terms of the transformed potentials Φ and Ψ as

$$\Phi_{yy}-(\alpha^2-k^2)\Phi=0, \text{ and } \Psi_{yy}-(\alpha^2-K^2)\Psi=0, \tag{13}$$

respectively. We assume that α lies in a strip $\mathscr{D}$, of finite width, which also encloses the integration contour $\mathscr{C}$. The region in the α-plane above and including $\mathscr{D}$, is denoted $\mathscr{D}_+$, whereas $\mathscr{D}_-$ occupies the half-plane below and including $\mathscr{D}$.

The solutions of Eqs. (13) which satisfy the radiation condition (i.e. purely outgoing waves or decaying solutions as $y\to\infty$) are of the form

$$\Phi(\alpha,y)=A(\alpha)\mathrm{e}^{-\gamma(\alpha)y}, \quad \Psi(\alpha,y)=B(\alpha)\mathrm{e}^{-\delta(\alpha)y}, \tag{14}$$

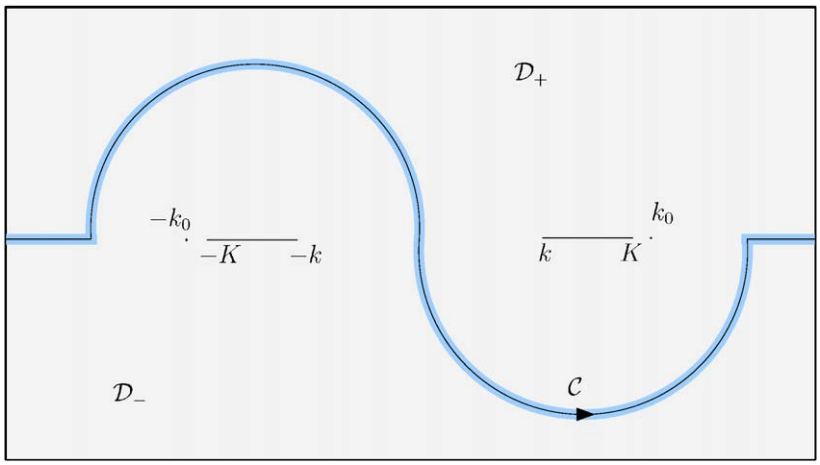

Fig. 2. The contour $\mathscr{C}$ in the complex α-plane, deformed away from the branch cuts and the Rayleigh poles, $\pm k_0$.

where the functions

$$\gamma(\alpha) = \sqrt{\alpha^2 - k^2} \quad \text{and} \quad \delta(\alpha) = \sqrt{\alpha^2 - K^2} \tag{15}$$

are defined on the complex plane, $\mathbb{C}$, cut from $\pm k$ to $\pm\infty$ and from $\pm K$ to $\pm\infty$ respectively. The Riemann sheets on which these functions are defined are chosen such that $\gamma(0) = -\mathrm{i}k$, $\delta(0) = -\mathrm{i}K$ and $\gamma/|\alpha| \to 1$, $\delta/|\alpha| \to 1$ as $|\alpha| \to \infty$ on $\mathbb{C}$. As shown in Ref. [16], the choice of these Riemann sheets is necessary to satisfy the Sommerfeld radiation condition.

Applying the Fourier transform to the displacement boundary condition Eq. (8) gives

$$\mathrm{e}^{\mathrm{i}\alpha l}\mathbf{U}_+ + \mathbf{U}_0 + \mathrm{e}^{-\mathrm{i}\alpha l}\mathbf{U}_- = \begin{pmatrix} -\mathrm{i}\alpha & -\delta \\ \gamma & -\mathrm{i}\alpha \end{pmatrix}\begin{pmatrix} A \\ B \end{pmatrix}, \tag{16}$$

where the vector functions

$$\mathbf{U}_+ = \int_l^\infty \mathrm{e}^{\mathrm{i}\alpha(x-l)}\begin{pmatrix} u(x,0) \\ -v(x,0) \end{pmatrix}\mathrm{d}x, \quad \mathbf{U}_- = \int_{-\infty}^{-l} \mathrm{e}^{\mathrm{i}\alpha(x+l)}\begin{pmatrix} u(x,0) \\ -v(x,0) \end{pmatrix}\mathrm{d}x \tag{17}$$

are as yet unknown and

$$\mathbf{U}_0 = \int_{-l}^{l} \mathrm{e}^{\mathrm{i}\alpha l}\begin{pmatrix} u_0(x) \\ -v_0(x) \end{pmatrix}\mathrm{d}x. \tag{18}$$

It can be shown from the properties of such half-line integral transforms with finite displacements (u, v) at $x = \pm l$, that functions with the $+$ and $-$ subscripts are analytic and of algebraic growth in $\mathscr{D}_+$ and $\mathscr{D}_-$, respectively, (see Ref. [11, Chapter 1]). The vector function $\mathbf{U}_0$ is entire in α. Transforming the stress free boundary conditions (Eqs. (9) and (10)) gives the vector equation

$$\mathbf{\Sigma}_1 = \frac{1}{\mu}\begin{pmatrix} \Sigma_{22}^1 \\ \Sigma_{12}^1 \end{pmatrix} = \begin{pmatrix} 2\alpha^2 - K^2 & -2\mathrm{i}\alpha\delta \\ 2\mathrm{i}\alpha\gamma & 2\alpha^2 - K^2 \end{pmatrix}\begin{pmatrix} A \\ B \end{pmatrix}, \tag{19}$$

where the entire functions Σ_{ij}^1 are the Fourier transforms of the normal (σ_{22}) and tangential (σ_{12}) stress on $y = 0$, given by

$$\Sigma_{ij}^1(\alpha) = \int_{-l}^{l} \mathrm{e}^{\mathrm{i}\alpha x}\sigma_{ij}(x,0)\,\mathrm{d}x. \tag{20}$$

Eliminating A and B from Eqs. (16) and (19) gives the modified, matrix Wiener–Hopf equation

$$\mathrm{e}^{\mathrm{i}\alpha l}\mathbf{U}_+ + \mathbf{K}\mathbf{\Sigma}_1 + \mathrm{e}^{-\mathrm{i}\alpha l}\mathbf{U}_- + \mathbf{U}_0 = 0, \tag{21}$$

with the matrix kernel $\mathbf{K}(\alpha)$ given by

$$\mathbf{K} = \frac{1}{R(\alpha)}\begin{pmatrix} \mathrm{i}\alpha(2\alpha^2 - K^2 - 2\gamma\delta) & -K^2\delta \\ K^2\gamma & \mathrm{i}\alpha(2\alpha^2 - K^2 - 2\gamma\delta) \end{pmatrix}, \tag{22}$$

where $R(\alpha)$ is the Rayleigh determinant,

$$R(\alpha) = (2\alpha^2 - K^2)^2 - 4\alpha^2\gamma\delta. \tag{23}$$

Eq. (21) is a so-called *modified* Wiener–Hopf equation as the kernel $\mathbf{K}$ multiplies an entire function, $\mathbf{\Sigma}_1$, rather than one that is analytic in only one half-plane. Note that $R(\alpha)$ has exactly two zeros, $\pm k_0$, in the α-plane cut as shown in Fig. 2, and that these zeros lie on the real line with $|\alpha| > K$. Their location corresponds to the wavenumbers of the Rayleigh waves which may propagate along the free surface of the body. Note also that the inverse matrix

$$\mathbf{K}^{-1} = \frac{1}{\alpha^2 - \gamma\delta}\begin{pmatrix} \mathrm{i}\alpha(2\alpha^2 - K^2 - 2\gamma\delta) & K^2\delta \\ -K^2\gamma & \mathrm{i}\alpha(2\alpha^2 - K^2 - 2\gamma\delta) \end{pmatrix} \tag{24}$$

has no poles on the chosen Riemann surface, corresponding to the fact that no surface waves are supported on the interface between the elastic body and our model transducer.

4. Factorization of the matrix kernel

It is now necessary to perform a Wiener–Hopf product factorization on the matrix $\mathbf{K}(\alpha)$, that is, to reduce it to a product $\mathbf{K}_+(\alpha)\mathbf{K}_-(\alpha)$ where $\mathbf{K}_+(\alpha)$, $\mathbf{K}_-(\alpha)$ (and their respective inverses) are analytic and of algebraic growth in overlapping upper and lower half planes, respectively. At present, there is no known method for performing this decomposition exactly. However, using a method due to Abrahams [12,13], it is possible to perform an approximate factorization.

The procedure for this approximate factorization proceeds in three steps. Firstly, a commutative factorization is obtained by the Khrapkov–Daniele [17,18] method. This factorization is exact, but the factors do not have the desired analyticity properties. Secondly, a specific scalar factor in this commutative factorization is replaced with its Padé approximant. Finally, these approximate factors are multiplied by meromorphic matrices defined such that each of the factors has poles only in one half-plane. This determines explicit but approximate expressions for $\mathbf{K}_\pm(\alpha)$, of arbitrary accuracy in $\mathscr{D}_\pm$.

For convenience the exact factorization of the matrix kernel $\mathbf{K}$ is performed by first factorising the matrix $\mathbf{L} = -\mathbf{K}\mathbf{J} = \mathbf{L}_+\mathbf{L}_-$, where

$$\mathbf{J} = \begin{pmatrix} 0 & -f(\alpha) \\ 1/f(\alpha) & 0 \end{pmatrix} \quad \text{and} \quad f(\alpha) = \sqrt{\frac{\delta(\alpha)}{\gamma(\alpha)}}. \tag{25}$$

We write each of the factors $\mathbf{L}_\pm$ in the form

$$\mathbf{L}_\pm = r_\pm(\alpha)(\cos(s_\pm(\alpha))\mathbf{I} + \sin(s_\pm(\alpha))\mathbf{J}), \tag{26}$$

where $\mathbf{I}$ is the 2×2 identity matrix and explicitly multiply $\mathbf{L}_+\mathbf{L}_-$. Comparing coefficients of $\mathbf{I}$ and $\mathbf{J}$ it is simple to derive the pair of scalar relationships

$$s_+ + s_- = -\tan^{-1}\left(\frac{\mathrm{i}\alpha(2\alpha^2 - K^2 - 2\gamma(\alpha)\delta(\alpha))}{K^2\sqrt{\gamma(\alpha)\delta(\alpha)}}\right), \tag{27}$$

$$[r_+r_-]^2 = \frac{\gamma(\alpha)\delta(\alpha) - \alpha^2}{R(\alpha)}. \tag{28}$$

We may now perform the standard scalar Wiener–Hopf decompositions for r_+, r_-, s_+ and s_-, in an identical manner to Ref. [12], to derive explicit expressions for the kernel factors. Choosing a symmetric factorization gives

$$\begin{aligned} r_+(\alpha) &= r_-(-\alpha) \\ &= \sqrt[4]{\frac{K^2 + k^2}{4(K^2 - k^2)}}\frac{\mathrm{e}^{-\mathrm{i}\pi/4}}{(\alpha + k_0)^{1/2}}\exp\left\{\frac{1}{4\pi\mathrm{i}}\int_{-K}^{-k}\log\left[\frac{S(\xi)(\xi^2 - \gamma\delta)}{R(\xi)(\xi^2 + \gamma\delta)}\right]\frac{\mathrm{d}\xi}{\xi - \alpha}\right\} \end{aligned} \tag{29}$$

and

$$s_+(\alpha) = -\frac{\alpha}{2\pi\mathrm{i}}\int_{\smile}\tan^{-1}\left[\frac{\mathrm{i}\xi(2\xi^2 - K^2 - 2\gamma\delta)}{K^2\sqrt{\gamma\delta}}\right]\frac{\mathrm{d}\xi}{\xi(\xi - \alpha)} = -s_-(-\alpha), \tag{30}$$

where $S(\xi) = (2\xi^2 - K^2)^2 + 4\xi^2\gamma(\xi)\delta(\xi)$ is the non-physical Rayleigh determinant and the contour $\smile$ denotes an integration path in $\mathscr{D}$ deformed so as to pass below α. The functions defined by these integrals may be easily calculated numerically for any given value of α.

The exact factorization above is not complete, in that $\mathbf{L}_{\pm}(\alpha)$ both contain the finite cuts of $f(\alpha)$ shown in Fig. 2. We may construct approximate kernel factors

$$\mathbf{L}_{N\pm} = r_{\pm}(\alpha)(\cos(s_{\pm}(\alpha))\mathbf{I} + \sin(s_{\pm}(\alpha))\mathbf{J}_N), \quad \mathbf{J}_N = \begin{pmatrix} 0 & -f_N \\ 1/f_N & 0 \end{pmatrix}, \tag{31}$$

where $f_N(\alpha)$ is a two-point $[2N/2N]$ Padé approximant of $f(\alpha)$, centred around $\alpha = 0$ and $\alpha = \infty$. Such two point approximants are used in order to guarantee that $f_N(\alpha)$ has the same asymptotic behaviour as $f(\alpha)$ for large α. Further properties of Padé approximants may be found in Baker and Graves-Morris [19, Chapter 7.1] and specific reference to two-point approximants is made in Abrahams [20]. Thus, since $f(\alpha) \to 1$ as $\alpha \to \infty$,

$$f_N(\alpha) = \frac{\prod_{n=0}^{N}(\alpha^2 - p_n^2)}{\prod_{n=0}^{N}(\alpha^2 - q_n^2)} \simeq \sqrt{\frac{\delta(\alpha)}{\gamma(\alpha)}}, \tag{32}$$

where the positive poles (q_n) and positive zeros (p_n) of f_N lie on the real line between k and K. So, if we define the approximate factors of $\mathbf{K}$ by

$$\widetilde{\mathbf{K}}_{N+} = \mathbf{L}_{N+}, \quad \widetilde{\mathbf{K}}_{N-} = \mathbf{L}_{N-}\mathbf{J}_N \tag{33}$$

then $\widetilde{\mathbf{K}}_{N+}$ (respectively, $\widetilde{\mathbf{K}}_{N-}$) and its inverse are analytic in $\mathscr{D}_+$ ($\mathscr{D}_-$) except for poles at p_n and q_n ($-p_n$ and $-q_n$).

The final step in the approximate Wiener–Hopf factorization is to construct a meromorphic matrix $\mathbf{M}$ such that $\widetilde{\mathbf{K}}_{N+}\mathbf{M}$ and $\mathbf{M}^{-1}\widetilde{\mathbf{K}}_{N-}$ are free of poles in $\mathscr{D}_+$ and $\mathscr{D}_-$ respectively. It is due to this step that the resulting approximate factorization is non-commutative. In order to generate such a matrix $\mathbf{M}$, we take the ansatz

$$\mathbf{M} = \begin{pmatrix} 1 + \sum_{n=1}^{N} \dfrac{A_n}{\alpha - q_n} + \sum_{n=1}^{N} \dfrac{B_n}{\alpha + q_n} & \sum_{n=1}^{N} \dfrac{\overline{A}_n}{\alpha - q_n} + \sum_{n=1}^{N} \dfrac{\overline{B}_n}{\alpha + q_n} \\ \sum_{n=1}^{N} \dfrac{C_n}{\alpha - p_n} + \sum_{n=1}^{N} \dfrac{D_n}{\alpha + p_n} & 1 + \sum_{n=1}^{N} \dfrac{\overline{C}_n}{\alpha - p_n} + \sum_{n=1}^{N} \dfrac{\overline{D}_n}{\alpha + p_n} \end{pmatrix}, \tag{34}$$

which may be derived using the procedure given in Ref. [12]). For the desired analyticity properties, we require the residue of the poles at p_n and q_n in each of the elements of $\mathbf{K}_{N+}$ to vanish, as must the residues of the poles at $-p_n$ and $-q_n$ in the elements of $\mathbf{K}_{N-}^{-1}$. Imposition of this condition creates a system of $8N$ algebraic equations for the $8N$ unknowns in the matrix $\mathbf{M}$ (i.e. the coefficients $A_1, ..., D_n, \overline{A}_1, ..., \overline{D}_n$.) It can be confirmed that this choice of coefficients also guarantees that $\mathbf{K}_{N+}^{-1}$ and $\mathbf{K}_{N-}$ are similarly free of poles in $\mathscr{D}_+$ and $\mathscr{D}_-$ respectively. Finally it can be shown that $|\mathbf{M}| = 1$ and so $|\mathbf{K}_{N\pm}| = r_{\pm}^2(\alpha)$ is independent of N.

In summary, explicit non-commutative factors of the Wiener–Hopf kernel function $\mathbf{K}(\alpha)$ have been obtained in this section. They are

$$\mathbf{K}(\alpha) \simeq \mathbf{K}_{N+}(\alpha)\mathbf{K}_{N-}(\alpha), \tag{35}$$

where

$$\mathbf{K}_{N+} = \mathbf{L}_{N+}\mathbf{M}, \quad \mathbf{K}_{N-} = \mathbf{M}^{-1}\mathbf{L}_{N-}. \tag{36}$$

Note that $\mathbf{K}_{N+}$ gives an accurate approximation to the exact factor $\mathbf{K}_+$ in $\mathscr{D}_+$, but not near the singularities in $\mathscr{D}_-$. If $\mathbf{K}_{N+}$ is required in $\mathscr{D}_-$ then it is appropriate to write

$$\mathbf{K}_+(\alpha) \simeq \mathbf{K}(\alpha)\mathbf{K}_{N-}^{-1}(\alpha), \quad \alpha \in \mathscr{D}_-, \tag{37}$$

where the singularities in $\mathscr{D}_-$ have not been approximated. Similarly, $\mathbf{K}_- \simeq \mathbf{K}_{N+}^{-1}\mathbf{K}$, $\alpha \in \mathscr{D}_+$. In the following sections the details and method of approximation are not relevant to the analysis, and any alternative product decomposition may be utilised. Thus the subscript N on the kernel factors will be omitted.

5. Solution of the boundary value problem

Having thus obtained an approximate matrix kernel decomposition, it is now possible to solve the modified Wiener–Hopf equation in the manner proposed by Jones [15]. Pre-multiplying Eq. (21) by $\mathrm{e}^{-\mathrm{i}\alpha l}\mathbf{K}_+^{-1}$ and

performing a Wiener–Hopf sum decomposition on each of the terms, gives

$$\mathbf{K}_+^{-1}\mathbf{U}_+ + [\mathrm{e}^{-2\mathrm{i}\alpha l}\mathbf{K}_+^{-1}\mathbf{U}_-]_+ + [\mathrm{e}^{-\mathrm{i}\alpha l}\mathbf{K}_+^{-1}\mathbf{U}_0]_+ = -\mathrm{e}^{-\mathrm{i}\alpha l}\mathbf{K}_-\boldsymbol{\Sigma}_1 - [\mathrm{e}^{-2\mathrm{i}\alpha l}\mathbf{K}_+^{-1}\mathbf{U}_-]_- - [\mathrm{e}^{-\mathrm{i}\alpha l}\mathbf{K}_+^{-1}\mathbf{U}_0]_-, \tag{38}$$

where $[\ ]_\pm$ denotes the part of the sum decomposition analytic in $\mathscr{D}_\pm$, respectively.

By construction, the left-hand side of Eq. (38) is analytic and of algebraic growth in $\mathscr{D}_+$ and the right-hand side is analytic and of algebraic growth in $\mathscr{D}_-$. Hence, each side of Eq. (38) is the analytic continuation of some function $\mathbf{E}$ which is entire and of algebraic growth in all of $\mathbb{C}$. Thus, by the extended form of Liouville's theorem, each side is identical to a vector of polynomials. Consideration of the asymptotic behaviour of the terms of Eq. (38) as $|\alpha| \to \infty$ (deduced from the local stress and displacement fields around the edges of the transducer as discussed in Ref. [12]) shows that $\mathbf{E} \to \mathbf{0}$, and hence $\mathbf{E} \equiv \mathbf{0}$. Rewriting Eq. (38) using the standard Wiener–Hopf decomposition formula, leaves us with an vector integral equation for $\mathbf{U}_+$ in terms of $\mathbf{U}_-$ and $\mathbf{U}_0$, i.e.

$$\mathbf{K}_+^{-1}\mathbf{U}_+ + \frac{1}{2\pi\mathrm{i}}\int_{\smile} [\mathrm{e}^{-2\mathrm{i}\xi l}\mathbf{K}_+^{-1}(\xi)\mathbf{U}_-(\xi) + \mathrm{e}^{-\mathrm{i}\xi l}\mathbf{K}_+^{-1}(\xi)\mathbf{U}_0(\xi)]\frac{\mathrm{d}\xi}{\xi-\alpha} = \mathbf{0}. \tag{39}$$

It is convenient to consider the arbitrary forcing in terms of functions which are odd or even in x and use the symmetry of the problem to rewrite $\mathbf{U}_-$ in terms of $\mathbf{U}_+$. We shall consider the case where the forcing is by a rigid transducer performing harmonic motion in the y direction only, i.e. $(u_0, v_0) = (0, -1)$, and so

$$\mathbf{U}_0(\alpha) = \int_{-l}^{l} \mathrm{e}^{\mathrm{i}\alpha x}\begin{pmatrix}0\\1\end{pmatrix}\mathrm{d}x = \frac{\mathrm{e}^{\mathrm{i}\alpha l} - \mathrm{e}^{-\mathrm{i}\alpha l}}{\mathrm{i}\alpha}\begin{pmatrix}0\\1\end{pmatrix}. \tag{40}$$

From the symmetry of the forcing and the body, it is seen that $u(x, y) = -u(-x, y)$, and $v(x, y) = v(-x, y)$, and thus

$$\mathbf{U}_-(\alpha) = \begin{pmatrix}-1 & 0\\ 0 & 1\end{pmatrix}\mathbf{U}_+(-\alpha). \tag{41}$$

For a given forcing it is frequently possible to perform partially an explicit Wiener–Hopf sum decomposition. In this case we may write the final term on the left-hand side of Eq. (39) as

$$\frac{1}{2\pi\mathrm{i}}\int_{\smile} \mathrm{e}^{-\mathrm{i}\xi l}\mathbf{K}_+^{-1}(\xi)\mathbf{U}_0(\xi)\frac{\mathrm{d}\xi}{\xi-\alpha} = \int_{\smile} \frac{\mathrm{e}^{-2\mathrm{i}\xi l}-1}{2\pi\xi}\mathbf{K}_+^{-1}(\xi)\begin{pmatrix}0\\1\end{pmatrix}\frac{\mathrm{d}\xi}{\xi-\alpha}$$
$$= \int_{\mathscr{C}_K\cup\mathscr{C}_k} \frac{\mathrm{e}^{-2\mathrm{i}\xi l}}{2\pi\xi}\mathbf{K}_+^{-1}(\xi)\begin{pmatrix}0\\1\end{pmatrix}\frac{\mathrm{d}\xi}{\xi-\alpha} - \frac{\mathrm{i}}{\alpha}\{\mathbf{K}_+^{-1}(\alpha) - \mathbf{K}_+^{-1}(0)\}\begin{pmatrix}0\\1\end{pmatrix}, \tag{42}$$

with the integral taken around the cuts from $-k$ and $-K$ parallel to the imaginary axis in the lower half-plane (as shown in Fig. 3). Here the contour $\mathscr{C}$ has been deformed onto a large semi-circular arc in the lower half

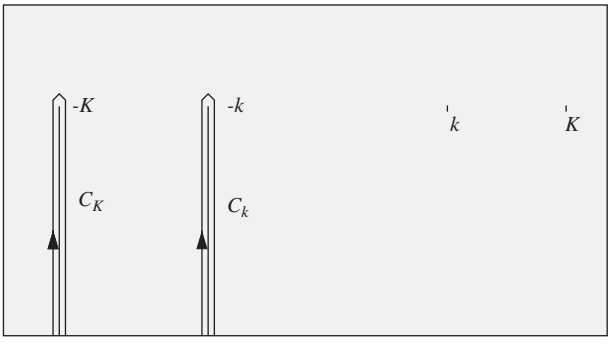

Fig. 3. Integration contour for Wiener–Hopf decomposition of $\mathbf{U}_0$.

plane (plus indentations around the two branch-cuts) whose contribution to the total integral can, by Jordan's Lemma, be shown to tend to zero as the radius of the semi-circle increases. Further, by noting that $\mathbf{K}_+^{-1} = \mathbf{K}_-\mathbf{K}^{-1}$ and that $\mathbf{K}^{-1}$ is free of poles, it can be seen that $\mathbf{K}_+^{-1}$ is similarly pole-free, containing only branch-cuts in the lower half-plane, $\mathscr{D}_-$.

Substituting Eqs. (41) and (42) into Eq. (39) and deforming the integration contour of the second term onto the path in Fig. 3, gives us an integral equation for $\mathbf{U}_+$, valid for all k, l, the solution of which will solve the boundary value problem. Thus,

$$\mathbf{K}_+^{-1}\mathbf{U}_+ + \frac{1}{2\pi \mathrm{i}}\int_{\mathscr{C}_k\cup\mathscr{C}_K} \mathrm{e}^{-2\mathrm{i}\xi l}\mathbf{K}_+^{-1}(\xi)\begin{pmatrix}-1 & 0\\ 0 & 1\end{pmatrix}\mathbf{U}_+(-\xi)\frac{\mathrm{d}\xi}{\xi-\alpha} = \frac{\mathrm{i}}{\alpha}\{\mathbf{K}_+^{-1}(\alpha)-\mathbf{K}_+^{-1}(0)\}\begin{pmatrix}0\\1\end{pmatrix} - \int_{\mathscr{C}_k\cup\mathscr{C}_K}\frac{\mathrm{e}^{-2\mathrm{i}\xi l}}{2\pi\xi}\mathbf{K}_+^{-1}(\xi)\frac{\mathrm{d}\xi}{\xi-\alpha}\begin{pmatrix}0\\1\end{pmatrix}. \tag{43}$$

In order to generate a solution for this equation, we shall make the assumption that $kl \gg 1$, which is to say that the transducer is long compared to a typical wavelength of the compressional body waves. Furthermore, denoting $\sqrt{kl} = \varepsilon^{-1}$, we may rewrite the potential as an asymptotic series in the small parameter, ε. Assuming the solution may be expressed as a perturbation expansion in the standard form, we write

$$\mathbf{U}_+ = \mathbf{U}_+^{(0)} + \varepsilon\mathbf{U}_+^{(1)} + \cdots + \varepsilon^n\mathbf{U}_+^{(n)} + \cdots, \tag{44}$$

and express the other unknowns with a similar notation. We may now rewrite the integral terms in Eq. (43) in terms of the small parameter. Approximating the integrands in the neighbourhood of $-k$ and $-K$ by their Taylor series expansions about these points we may write each of the integrals in the form

$$\int_{\mathscr{C}_k}\mathrm{e}^{-2\mathrm{i}\xi l}\mathbf{K}_+^{-1}(\xi)\mathbf{f}(\boldsymbol{\xi})\frac{\mathrm{d}\xi}{\xi-\alpha} = \varepsilon^3\mathbf{P}_0\mathbf{f}(-k)\ F\left(\frac{\alpha+k}{k}\right) + O(\varepsilon^4), \tag{45}$$

where $\mathbf{P}_0$ is a constant matrix. For clarity of presentation, the elements of $\mathbf{P}_0$ and details of the derivation are left for the appendix (see Eqs. (A.1)–(A.12)). A similar expression is derived for the integral over contour $\mathscr{C}_K$. Note that since the region $\mathscr{D}$ is indented away from $-k$ and $-K$, the function F, given in the appendix (Eq. (A.9)), is $O(\varepsilon^0)$ in that region.

Eq. (45) is valid in the domain $\mathscr{D}$ containing the contour $\mathscr{C}$ over which the inverse Fourier integrals are taken. Thus, the contribution to Eq. (43) from the integrals around the branch cuts is $O(\varepsilon^3)$, whereas that from the pole contribution is $O(\varepsilon^0)$. Therefore we may substitute our asymptotic expression for $\mathbf{U}_+$ and generate an approximate solution to the integral equation by collecting terms in coefficients of ε^n. Substituting Eq. (44) into Eq. (43) and considering only the coefficient of ε^0 gives us, as the first approximation to the solution

$$\mathbf{K}_+^{-1}(\alpha)\mathbf{U}_+^{(0)}(\alpha) = \frac{\mathrm{i}}{\alpha}\{\mathbf{K}_+^{-1}(\alpha)-\mathbf{K}_+^{-1}(0)\}\begin{pmatrix}0\\1\end{pmatrix}. \tag{46}$$

We may now calculate $\mathbf{U}_+^{(0)}(k)$ and $\mathbf{U}_+^{(0)}(K)$ explicitly, and use these to derive the next term in the asymptotic series. By comparing the coefficients of powers of ε, ε^2 and ε^3 we obtain further terms in the expansion. Thus,

$$\mathbf{K}_+^{-1}(\alpha)\mathbf{U}_+^{(1)}(\alpha) = \mathbf{K}_+^{-1}(\alpha)\mathbf{U}_+^{(2)}(\alpha) \equiv \mathbf{0} \tag{47}$$

and

$$\mathbf{K}_+^{-1}(\alpha)\mathbf{U}_+^{(3)}(\alpha) = \frac{1}{2\pi k}F\left(\frac{\alpha+k}{k}\right)\mathbf{P}_0\begin{pmatrix}-1 & 0\\ 0 & 1\end{pmatrix}\mathbf{K}_+(k)\mathbf{K}_+^{-1}(0)\begin{pmatrix}0\\1\end{pmatrix} + \frac{1}{2\pi K}F\left(\frac{\alpha+K}{k}\right)\mathbf{P}_1\begin{pmatrix}-1 & 0\\ 0 & 1\end{pmatrix}\mathbf{K}_+(K)\mathbf{K}_+^{-1}(0)\begin{pmatrix}0\\1\end{pmatrix}, \tag{48}$$

where the constant matrices $\mathbf{P}_0$ and $\mathbf{P}_1$ are given in Eq. (A.12). In principle, any degree of accuracy may be obtained: $\mathbf{U}_+^{(n)}$ may be used in the iteration procedure to generate higher order terms.

Having thus constructed the first two non-zero terms in the asymptotic expansion Eq. (44), and outlined a scheme to generate further terms to arbitrary accuracy, all that remains is to obtain the potential functions ϕ and ψ using the inverse Fourier transforms given in Eqs. (11) and (12). From Eqs. (14) and (16),

$$\begin{pmatrix} \Phi \\ \Psi \end{pmatrix} = \begin{pmatrix} A\mathrm{e}^{-\gamma y} \\ B\mathrm{e}^{-\delta y} \end{pmatrix}, \tag{49}$$

where

$$\begin{pmatrix} A \\ B \end{pmatrix} = \frac{1}{\alpha^2 - \gamma\delta} \begin{pmatrix} \mathrm{i}\alpha & -\delta \\ \gamma & \mathrm{i}\alpha \end{pmatrix} \{\mathrm{e}^{\mathrm{i}\alpha l}\mathbf{U}_+(\alpha) + \mathbf{U}_0(\alpha) + \mathrm{e}^{-\mathrm{i}\alpha l}\mathbf{U}_-(\alpha)\} \tag{50}$$

and we may define $\Phi^{(n)}$, $\Psi^{(n)}$ by

$$\begin{pmatrix} \Phi^{(n)} \\ \Psi^{(n)} \end{pmatrix} = \frac{1}{\alpha^2 - \gamma\delta} \begin{pmatrix} \mathrm{i}\alpha\mathrm{e}^{-\gamma y} & -\delta\mathrm{e}^{-\gamma y} \\ \gamma\mathrm{e}^{-\delta y} & \mathrm{i}\alpha\mathrm{e}^{-\delta y} \end{pmatrix} \{\mathrm{e}^{\mathrm{i}\alpha l}\mathbf{U}_+^{(n)}(\alpha) + \delta_{0n}\mathbf{U}_0 + \mathrm{e}^{-\mathrm{i}\alpha l}\mathbf{U}_-^{(n)}(\alpha)\}. \tag{51}$$

Hence, we can construct approximations to the solution by writing

$$\phi = \phi^{(0)} + \varepsilon\phi^{(1)} + \cdots + \varepsilon^n\phi^{(n)} + \cdots, \quad \phi^{(n)} = \frac{1}{2\pi}\int_{\mathscr{C}} \mathrm{e}^{-\mathrm{i}\alpha x}\Phi^{(n)}(\alpha, y)\,\mathrm{d}\alpha. \tag{52}$$

Note that since the steepest descent paths used to evaluate the $\phi^{(n)}$ need not remain in $\mathscr{D}$, the $\phi^{(n)}$ are not everywhere $O(\varepsilon^0)$ themselves. However, this does not cause problems for the analysis, since we require only that the $\Phi^{(n)}$ are $O(\varepsilon^0)$ for $\alpha \in \mathscr{D}$.

Taking the first term in the asymptotic series we calculate the first approximation to the potential ϕ by

$$\begin{aligned} \phi^{(0)}(x, y) &= \frac{1}{2\pi}\int_{\mathscr{C}} \frac{\mathrm{e}^{-\mathrm{i}\alpha x - \gamma y}}{\alpha^2 - \gamma\delta}(\mathrm{i}\alpha, -\delta)\{\mathrm{e}^{\mathrm{i}\alpha l}\mathbf{U}_+^{(0)}(\alpha) + \mathbf{U}_0(\alpha) + \mathrm{e}^{-\mathrm{i}\alpha l}\mathbf{U}_-^{(0)}(\alpha)\}\,\mathrm{d}\alpha \\ &= \frac{1}{2\pi\mathrm{i}}\int_{\mathscr{C}} \frac{\mathrm{e}^{-\mathrm{i}\alpha x - \gamma y}}{\alpha(\alpha^2 - \gamma\delta)}(\mathrm{i}\alpha, -\delta)\left\{\mathrm{e}^{\mathrm{i}\alpha l}\mathbf{K}_+(\alpha) + \mathrm{e}^{-\mathrm{i}\alpha l}\begin{pmatrix} 1 & 0 \\ 0 & -1 \end{pmatrix}\mathbf{K}_+(-\alpha)\right\}\mathbf{K}_+^{-1}(0)\begin{pmatrix} 0 \\ 1 \end{pmatrix}\mathrm{d}\alpha. \end{aligned} \tag{53}$$

This leading order solution is composed of the sum of the solutions to two boundary value problems involving semi-infinite transducers (i.e. the radiated field from each end) of the type solved in Ref. [12]. In order to derive a uniformly valid asymptotic expansion for the far-field form of ϕ we shall split Eq. (53) into three parts. Defining $\gamma_+(\alpha) = (\alpha + k)^{1/2}$ and $\gamma_-(\alpha) = (\alpha - k)^{1/2}$, with branches chosen such that $\gamma_+(\alpha)\gamma_-(\alpha) \equiv \gamma(\alpha)$, we have

$$\begin{aligned} \phi^{(0)} = &\frac{1}{2\pi\mathrm{i}}\int_{\mathscr{C}} \mathrm{e}^{-\mathrm{i}\alpha(x-l)-\gamma y}\left\{\frac{(\mathrm{i}\alpha, \quad -\delta)}{\alpha(\alpha^2 - \gamma\delta)}\mathbf{K}_+(\alpha)\mathbf{K}_+^{-1}(0)\begin{pmatrix} 0 \\ 1 \end{pmatrix} - \frac{1}{\alpha\gamma_+(0)\gamma_-(\alpha)}\right\}\mathrm{d}\alpha \\ &+ \frac{1}{2\pi\mathrm{i}}\int_{\mathscr{C}} \mathrm{e}^{-\mathrm{i}\alpha(x+l)-\gamma y}\left\{\frac{(\mathrm{i}\alpha, \ \delta)}{\alpha(\alpha^2 - \gamma\delta)}\mathbf{K}_+(-\alpha)\mathbf{K}_+^{-1}(0)\begin{pmatrix} 0 \\ 1 \end{pmatrix} + \frac{1}{\alpha\gamma_+(0)\gamma_-(-\alpha)}\right\}\mathrm{d}\alpha \\ &+ \frac{1}{2\pi\mathrm{i}\gamma_+(0)}\int_{\mathscr{C}} \mathrm{e}^{-\mathrm{i}\alpha x - \gamma y}\left\{\frac{\mathrm{e}^{\mathrm{i}\alpha l}}{\alpha\gamma_-(\alpha)} - \frac{\mathrm{e}^{-\mathrm{i}\alpha l}}{\alpha\gamma_-(-\alpha)}\right\}\mathrm{d}\alpha. \end{aligned} \tag{54}$$

The integrands in the first two integrals in Eq. (54) are bounded on the interval $(-k, k)$ in the complex plane and an asymptotic formula may be obtained using the method of steepest descent. Denoting the first integral as

$$\begin{aligned} \phi_l^{(0)}(x, y) &= \frac{1}{2\pi\mathrm{i}}\int_{\mathscr{C}} \mathrm{e}^{-\mathrm{i}\alpha(x-l)-\gamma y}\left\{\frac{(\mathrm{i}\alpha, \quad -\delta)}{\alpha(\alpha^2 - \gamma\delta)}\mathbf{K}_+(\alpha)\mathbf{K}_+^{-1}(0)\begin{pmatrix} 0 \\ 1 \end{pmatrix} - \frac{1}{\alpha\gamma_+(0)\gamma_-(\alpha)}\right\}\mathrm{d}\alpha \\ &= \frac{1}{2\pi\mathrm{i}}\int_{\mathscr{C}} \mathrm{e}^{-\mathrm{i}\alpha(x-l)-\gamma y} f(\alpha)\,\mathrm{d}\alpha, \end{aligned} \tag{55}$$

it may be evaluated asymptotically by using plane polar coordinates centred on $x = l$, $y = 0$ as shown in Fig. 4. (Here and henceforth $\phi_{\pm l}$, $\psi_{\pm l}$ indicate the contribution to the respective potentials from the cylindrical

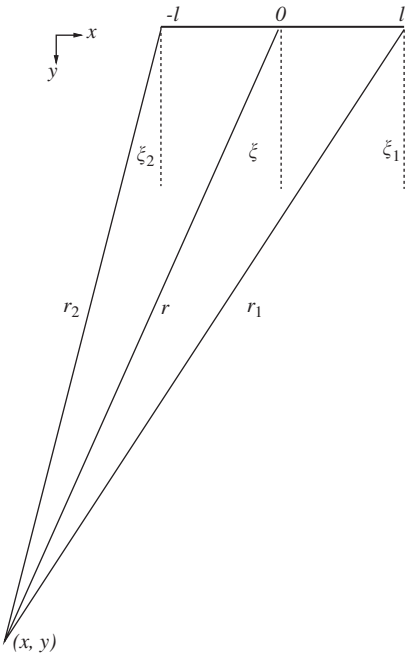

Fig. 4. Polar coordinates r_1, r_2, r, ξ_1, ξ_2 and ξ.

waves generated at the edges $x = \pm l$.) We therefore write

$$x - l = -r_1 \sin\xi_1, \quad y = r_1 \cos\xi_1, \tag{56}$$

and deform the contour $\mathscr{C}$ onto the half-parabola given parametrically by $\alpha = k\sin(\xi_1 + \mathrm{i}t)$ for $-\infty < t < \infty$. Without loss of generality we make the assumption that no singularities in $f(\alpha)$ are encountered during such a deformation. Hence, making the change of variable $\alpha = k\sin(\xi_1 + \mathrm{i}t)$ in the integrand gives

$$\int_{\mathscr{C}} f(\alpha)\mathrm{e}^{-\mathrm{i}\alpha(x-l)-\gamma y}\mathrm{d}\alpha = -\mathrm{i}k\int_{-\infty}^{\infty} \cos(\xi_1 + \mathrm{i}t) f(k\sin(\xi_1 + \mathrm{i}t))\mathrm{e}^{\mathrm{i}kr_1\cosh t}\mathrm{d}t, \tag{57}$$

and assuming that $kr_1 \gg 1$, we may now apply the method of stationary phase to obtain the asymptotic formula

$$\int_{\mathscr{C}} f(\alpha)\mathrm{e}^{-\mathrm{i}\alpha(x-l)-\gamma y}\mathrm{d}\alpha \sim -\mathrm{i}k\cos\xi_1 f(k\sin\xi_1)\sqrt{\frac{2\pi}{kr_1}}\mathrm{e}^{\mathrm{i}kr_1+\mathrm{i}\pi/4}, \tag{58}$$

and thus,

$$\phi_l^{(0)}(r_1,\xi_1) \sim -\frac{k\cos\xi_1}{\sqrt{2\pi kr_1}}\mathrm{e}^{\mathrm{i}kr_1+\mathrm{i}\pi/4} f(k\sin\xi_1). \tag{59}$$

Similarly, writing

$$x + l = -r_2\sin\xi_2, \quad y = r_2\cos\xi_2, \tag{60}$$

it can be seen from the symmetry, that the second integral in Eq. (54) becomes

$$\frac{1}{2\pi\mathrm{i}}\int_{\mathscr{C}} \mathrm{e}^{-\mathrm{i}\alpha(x+l)-\gamma y}\left\{\frac{(\mathrm{i}\alpha, \quad \delta)}{\alpha(\alpha^2-\gamma\delta)}\mathbf{K}_+(-\alpha)\mathbf{K}_+^{-1}(0)\begin{pmatrix}0\\1\end{pmatrix} + \frac{1}{\alpha\gamma_+(0)\gamma_-(-\alpha)}\right\}\mathrm{d}\alpha$$
$$\sim -\frac{k\cos\xi_2}{\sqrt{2\pi kr_2}}\mathrm{e}^{\mathrm{i}kr_2+\mathrm{i}\pi/4} f(-k\sin\xi_2). \tag{61}$$

The final term in Eq. (54) may be evaluated analytically. The integral

$$I = \gamma_-(0) \int_{\mathscr{C}} \frac{\mathrm{e}^{-\mathrm{i}\alpha(x-l)-\gamma(\alpha)y}}{\alpha\gamma_-(\alpha)}\,\mathrm{d}\alpha, \tag{62}$$

where $\mathscr{C}$ is indented below the origin, can be shown (see Ref. [11, Chapter 1.6]) to be expressible as a sum of Fresnel functions in the form

$$I = 2\pi^{1/2}\mathrm{e}^{\mathrm{i}\pi/4}[\mathrm{e}^{\mathrm{i}ky}\mathscr{F}(-\sqrt{2kr_1}\,\sin\tfrac{1}{2}\xi_1) - \mathrm{e}^{-\mathrm{i}ky}\mathscr{F}(\sqrt{2kr_1}\,\cos\tfrac{1}{2}\xi_1)] \tag{63}$$

where $\mathscr{F}(z)$ is the complex Fresnel integral defined as

$$\mathscr{F}(z) = \int_z^\infty \mathrm{e}^{\mathrm{i}u^2}\,\mathrm{d}u. \tag{64}$$

Thus, using the identity

$$\mathscr{F}(z) + \mathscr{F}(-z) = \sqrt{\pi}\mathrm{e}^{\mathrm{i}\pi/4}, \tag{65}$$

we obtain the exact expression

$$\begin{aligned}\frac{1}{2\pi\mathrm{i}\gamma_+(0)}\int_{\mathscr{C}} \mathrm{e}^{-\mathrm{i}\alpha x-\gamma y}\left\{\frac{\mathrm{e}^{\mathrm{i}\alpha l}}{\alpha\gamma_-(\alpha)} - \frac{\mathrm{e}^{-\mathrm{i}\alpha l}}{\alpha\gamma_-(-\alpha)}\right\}\mathrm{d}\alpha = \frac{\mathrm{e}^{\mathrm{i}\pi/4}}{k\sqrt{\pi}}\{\mathrm{e}^{\mathrm{i}ky}(\mathscr{F}(\sqrt{2kr_2}\,\sin\tfrac{1}{2}\xi_2) - \mathscr{F}(\sqrt{2kr_1}\,\sin\tfrac{1}{2}\xi_1))\\ - \mathrm{e}^{-\mathrm{i}ky}(\mathscr{F}(\sqrt{2kr_2}\,\cos\tfrac{1}{2}\xi_2) + \mathscr{F}(\sqrt{2kr_1}\,\cos\tfrac{1}{2}\xi_1))\}.\end{aligned} \tag{66}$$

From the symmetry inherent in the model problem, it can be shown that the total potential is given by

$$\begin{aligned}\phi^{(0)} \sim & -\frac{k\mathrm{e}^{\mathrm{i}\pi/4}\cos\xi}{\sqrt{2\pi kr}}\mathrm{e}^{\mathrm{i}kr}\{\mathrm{e}^{\mathrm{i}kl\sin\xi}f(k\sin\xi) + \mathrm{e}^{-\mathrm{i}kl\sin\xi}f(-k\sin\xi)\}\\ & + \frac{\mathrm{e}^{\mathrm{i}ky}\mathrm{e}^{\mathrm{i}\pi/4}}{k\sqrt{\pi}}[\mathscr{F}(\sqrt{2kr_2}\,\sin\tfrac{1}{2}\xi_2) - \mathscr{F}(\sqrt{2kr_1}\,\sin\tfrac{1}{2}\xi_1)]\\ & - \frac{\mathrm{e}^{-\mathrm{i}ky}\mathrm{e}^{\mathrm{i}\pi/4}}{k\sqrt{\pi}}[\mathscr{F}(\sqrt{2kr_2}\,\cos\tfrac{1}{2}\xi_2) + \mathscr{F}(\sqrt{2kr_1}\,\cos\tfrac{1}{2}\xi_1)],\end{aligned} \tag{67}$$

where the radii r_1, r_2 and r and the angles ξ, ξ_1 and ξ_2 are as shown in Fig. 4. In the limit $kr \to \infty$ the final term in Eq. (67) may be approximated using the asymptotic expansion

$$\mathscr{F}(z) \sim \frac{\mathrm{i}}{2z}\mathrm{e}^{\mathrm{i}z^2} \quad \text{as } z \to \infty. \tag{68}$$

The middle term of Eq. (67) may be rewritten as

$$g(r,\xi) = \frac{\mathrm{e}^{\mathrm{i}ky}\mathrm{e}^{\mathrm{i}\pi/4}}{k\sqrt{\pi}}\int_{\sqrt{2kr_2}\,\sin\xi_2/2}^{\sqrt{2kr_1}\,\sin\xi_1/2} \mathrm{e}^{\mathrm{i}u^2}\,\mathrm{d}u, \tag{69}$$

which, in the limit $kr \to \infty$, can be shown to simplify to

$$g(r,\xi) \sim \frac{\sin(kl\sin\xi)}{\sin\frac{1}{2}\xi}\frac{\mathrm{e}^{\mathrm{i}kr}\mathrm{e}^{\mathrm{i}\pi/4}}{k\sqrt{2\pi kr}}. \tag{70}$$

Thus, the *leading order* approximation to the radiated wave field is given by the asymptotic expansion

$$\phi^{(0)} \sim \frac{\mathrm{e}^{\mathrm{i}kr}\mathrm{e}^{\mathrm{i}\pi/4}}{\sqrt{2\pi kr}}\left\{\frac{\sin(kl\sin\xi)}{k\sin\frac{1}{2}\xi} - \frac{\mathrm{i}\cos(kl\sin\xi)}{k\cos\frac{1}{2}\xi} - k\cos\xi[\mathrm{e}^{\mathrm{i}kl\sin\xi}f(k\sin\xi) + \mathrm{e}^{-\mathrm{i}kl\sin\xi}f(-k\sin\xi)]\right\}. \tag{71}$$

The first correction term, $\phi^{(3)}$ may be calculated in a similar fashion to that performed above. From Eq. (52) we have

$$\begin{aligned}\phi^{(3)} &= \frac{1}{2\pi}\int_{\mathscr{C}} \mathrm{e}^{-\mathrm{i}\alpha x}\Phi^{(3)}(\alpha, y)\,\mathrm{d}\alpha \\ &= \frac{1}{2\pi}\int_{\mathscr{C}} \frac{\mathrm{e}^{-\mathrm{i}\alpha x-\gamma y}}{\alpha^2-\gamma\delta}(\mathrm{i}\alpha,\ -\delta)\{\mathrm{e}^{\mathrm{i}\alpha l}\mathbf{U}_+^{(3)}(\alpha)+\mathrm{e}^{-\mathrm{i}\alpha l}\mathbf{U}_-^{(3)}(\alpha)\}\,\mathrm{d}\alpha. \end{aligned} \tag{72}$$

Considering only the cylindrical wave radiated from the edge of the transducer at $x = l$, i.e. the first term in curly brackets in Eq. (72), we obtain

$$\phi_l^{(3)} = \frac{1}{2\pi}\int_{\mathscr{C}} \frac{\mathrm{e}^{-\mathrm{i}\alpha(x-l)-\gamma y}}{\alpha^2-\gamma\delta}(\mathrm{i}\alpha,\ -\delta)\mathbf{U}_+^{(3)}(\alpha)\,\mathrm{d}\alpha, \tag{73}$$

and we may again apply the method of stationary phase to obtain the asymptotic formula

$$\phi_l^{(3)}(r,\theta) = \frac{(-\mathrm{i}k\cos\theta,\ -\delta(-k\cos\theta))}{k^2\cos^2\theta + k\sin\theta(K^2-k^2\cos^2\theta)^{1/2}}\frac{k\sin\theta}{\sqrt{2\pi kr}}\mathrm{e}^{\mathrm{i}kr-\mathrm{i}\pi/4}\mathbf{U}_+^{(3)}(-k\cos\theta), \tag{74}$$

where $\mathbf{U}_+^{(3)}(\alpha)$ is given in Eq. (48). From the asymptotic forms of $F(z)$ for large z (obtainable using the definition given in Eq. (A.9)), it can be shown that $\phi^{(3)}$ is $O(\varepsilon^0)$ for all θ except near $\theta = 0$, where it is $O(\varepsilon^{-2})$. It can be deduced directly from Eq. (74) by considering the symmetry in geometry and forcing that the contribution from $\phi^{(3)}$ to the cylindrical wave radiating from the left edge ($x = -l$) is given by

$$\phi_{-l}^{(3)}(r,\theta) = \phi_l^{(3)}(r,\pi-\theta). \tag{75}$$

Identical procedures may be used to derive successive approximations to $\psi(x, y)$, which give the results

$$\psi_l^{(0)} = \frac{(\gamma(-K\cos\theta),\ -\mathrm{i}K\cos\theta)}{K^2\cos^2\theta + \mathrm{i}K\sin\theta\gamma(-K\cos\theta)}\frac{\tan\theta}{\sqrt{2\pi Kr}}\mathrm{e}^{\mathrm{i}Kr+\mathrm{i}\pi/4}\mathbf{K}_+(-K\cos\theta)\mathbf{K}_+^{-1}(0)\begin{pmatrix}0\\1\end{pmatrix} \tag{76}$$

and

$$\psi_l^{(3)}(r,\theta) = \frac{(\gamma(-K\cos\theta),\ -\mathrm{i}K\cos\theta)}{K^2\cos^2\theta + \mathrm{i}K\sin\theta\gamma(-K\cos\theta)}\frac{K\sin\theta}{\sqrt{2\pi Kr}}\mathrm{e}^{\mathrm{i}Kr-\mathrm{i}\pi/4}\mathbf{U}_+^{(3)}(-K\cos\theta), \tag{77}$$

along with the symmetry relation

$$\psi^{(n)} = \psi_l^{(n)}(r,\theta) - \psi_l^{(n)}(r,\pi-\theta). \tag{78}$$

6. Waves generated by a transducer with arbitrary displacements

We may now consider the effect on the partition of energy into the different wave types, and the directivity pattern of the wave-field, of specifying a different displacement field on the surface of the transducer. For simplicity, we shall again restrict ourselves to symmetric boundary conditions only. Suppose, we impose the displacement

$$\begin{pmatrix}u(x,0)\\v(x,0)\end{pmatrix} = \begin{pmatrix}0\\g(x)\end{pmatrix}, \quad |x| < l, \tag{79}$$

where $g(x)$ is an even function. Since we have examined the constant displacement case in Section 5 we may assume, without loss of generality, that $f(l) = 0$. Thus, we may write $g(x)$ as a Fourier series in x, of the form

$$g(x) = \sum_{m=0}^{\infty} a_m \cos\left(\frac{(2m+1)\pi x}{2l}\right). \tag{80}$$

Due to the linearity of the governing equations and boundary conditions, the solution of the specified boundary value problem is given by the sum of the solutions for each of the sinusoidal forcings on the right-hand

side of Eq. (80) with appropriate weights a_m. We shall therefore solve the general case when $u_0 = 0$, $v_0 = \cos((2m+1)\pi x/2l)$.

Substituting these boundary conditions into Eq. (18), and performing the procedure outlined above we obtain the following expression for the first approximation to the transformed potential,

$$\begin{aligned}\mathbf{U}^{(0)} = \frac{\mathrm{i}}{2}\Bigg[&\frac{\mathrm{e}^{\mathrm{i}(\alpha l+n\pi/2)}}{\alpha+n\pi/2l}\mathbf{K}_+(\alpha)\mathbf{K}_+^{-1}\left(-\frac{n\pi}{2l}\right)\begin{pmatrix}0\\1\end{pmatrix}\\&+\frac{\mathrm{e}^{-\mathrm{i}(\alpha l+n\pi/2)}}{\alpha+n\pi/2l}\begin{pmatrix}1&0\\0&-1\end{pmatrix}\mathbf{K}_+(-\alpha)\mathbf{K}_+^{-1}\left(\frac{n\pi}{2l}\right)\begin{pmatrix}0\\1\end{pmatrix}\\&+\frac{\mathrm{e}^{-\mathrm{i}(\alpha l-n\pi/2)}}{\alpha-n\pi/2l}\begin{pmatrix}1&0\\0&-1\end{pmatrix}\mathbf{K}_+(-\alpha)\mathbf{K}_+^{-1}\left(-\frac{n\pi}{2l}\right)\begin{pmatrix}0\\1\end{pmatrix}\\&+\frac{\mathrm{e}^{\mathrm{i}(\alpha l-n\pi/2)}}{\alpha-n\pi/2l}\mathbf{K}_+(\alpha)\mathbf{K}_+^{-1}\left(\frac{n\pi}{2l}\right)\begin{pmatrix}0\\1\end{pmatrix}\Bigg],\end{aligned}\tag{81}$$

where $n = 2m+1$. This potential has removable singularities at $\alpha = \pm n\pi/2l$, and the solution takes different forms depending on whether the singularities lie in the interval $[-K, K]$. The locations of these singularities give the following separate cases:

6.1. $n\pi < 2kl$

When $n\pi < 2kl$ the removable singularities in $\mathbf{U}^{(0)}$, given in Eq. (81), lie in the interval $[-k, k]$, and the uniformly valid form of the far-field for both ϕ and ψ must be written in terms of Fresnel functions, found by employing the identity

$$\int_{\mathscr{C}}\frac{\sin(\alpha l - kl\cos\Theta)\exp(-\mathrm{i}\alpha x-\gamma y)}{\gamma_-(\alpha)(\alpha-k\cos\Theta)}\,\mathrm{d}\alpha = \mathrm{e}^{-\mathrm{i}kl\cos\Theta}\mathscr{G}(r,\theta) - \mathrm{e}^{\mathrm{i}kl\cos\Theta}\mathscr{G}(r,\theta),\tag{82}$$

where

$$\mathscr{G}(r,\theta) = \frac{\sqrt{\pi}\mathrm{e}^{-\mathrm{i}\pi/4}}{\gamma_-(k\cos\Theta)}\left[\mathrm{e}^{-\mathrm{i}kr\cos(\theta+\Theta)}\mathscr{F}\left(\sqrt{2kr}\cos\frac{1}{2}(\theta+\Theta)\right) - \mathrm{e}^{-\mathrm{i}kr\cos(\theta-\Theta)}\mathscr{F}\left(\sqrt{2kr}\cos\frac{1}{2}(\theta-\Theta)\right)\right]\tag{83}$$

and $\mathscr{F}(z)$ is the complex Fresnel function defined by Eq. (64).

Except in the special case when $n\pi$ is approximately $\pm 2kl$, the second term in Eq. (83) may be approximated, for large kr, using the asymptotic formula in Eq. (68). While the individual terms in Eq. (83) do not have uniform asymptotic expansions of order $(kr)^{-1/2}$, their difference is order $(kr)^{-1/2}$. In this case, this asymptotic formula is given by

$$\int_{\mathscr{C}}\frac{\sin(\alpha l - kl\cos\Theta)\exp(-\mathrm{i}\alpha x-\gamma y)}{(\alpha-k\cos\Theta)}\,\mathrm{d}\alpha \sim \mathrm{e}^{-\mathrm{i}\pi/4}\mathrm{e}^{\mathrm{i}kr}\sqrt{\frac{2\pi}{kr}}\sin\theta\,\frac{\sin(kl(\cos\theta+\cos\Theta))}{\cos\theta+\cos\Theta}.\tag{84}$$

The effect of this, therefore, is that the diffracted compressional and shear potentials (respectively, ϕ and ψ) are $O(\varepsilon^0)$ except in the vicinity of the critical angles, respectively $\pm\Theta_c$ and $\pm\Theta_s$, given by

$$\Theta_c = \arccos\frac{n\pi}{2kl} \quad \text{and} \quad \Theta_s = \arccos\frac{n\pi}{2Kl}.\tag{85}$$

6.2. $2Kl < n\pi$

For the case $n\pi > 2Kl$ the removable singularities in $\mathbf{U}^{(0)}$, given in Eq. (81), lie outside the interval $[-K, K]$ and are, therefore, not near the stationary phase point of the integral which defines the inverse Fourier transform. Thus, the approximation to the integral given by a direct application of the method of stationary phase is uniformly valid except near to grazing angles $\theta \approx 0, \pi$. At the grazing angle the steepest descent

contour passes near to the poles at $\pm n\pi/2l$ which, like the Rayleigh pole at $\pm k_0$, gives rise to outward travelling surface waves, whose magnitude decays exponentially in the y direction. However, for sufficiently large kr this exponential decay is so rapid that these contributions can be neglected at leading order.

6.3. $2kl < n\pi < 2Kl$

When $2kl < n\pi < 2Kl$ the removable singularities in $\mathbf{U}^{(0)}$, given in Eq. (81), lie in the intervals $[-K, -k]$ and $[k, K]$, and thus in the inversion integral for ψ this corresponds to a maximum in the wave field at the angle Θ_s given in Eq. (85). In the inversion integral for ϕ the singularity lies outside the possible range of values for the stationary phase point, and therefore, as in Eq. (6.2) above, the contribution from the pole is negligible.

6.4. Special cases

When the removable singularities at $\alpha = \pm n\pi/2l$ are very close to the branch cuts at $\pm k$ or $\pm K$ the nature of the singularities in the Fourier inversion integrals changes, and the stationary phase asymptotic analysis carried out above is no longer valid. In particular, for the case when $n\pi = 2kl$ the pole and the branch cut coalesce. If we consider the inversion integrals centred on $x = l$ and $-l$ separately, we find each integrand has an expansion in a neighbourhood of $\alpha = -k$, of the form

$$(\alpha + k)^{-1}\mathbf{c}_{-1} + (\alpha + k)^{-1/2}\mathbf{c}_{-1/2} + \mathbf{c}_0 + (\alpha + k)^{1/2}\mathbf{c}_{1/2} + \ldots, \tag{86}$$

where the vectors $\mathbf{c}_p$ are constant. Expansions for the two integrals must be derived separately.

For ϕ, the separate inversion integrals for ϕ_l and ϕ_{-l} each diverge as $\cos\theta_i$ approaches ± 1, but in this limit the stationary phase points for the two integral coincide at $\pm k$ and so the solution remains valid and bounded. Contribution from the order $(\alpha + k)^{-1/2}$ term may be calculated directly from the method of stationary phase, using Watson's Lemma.

For ψ the simple poles at $\pm k$ may be dealt with exactly as in case (6.1) above. The order $(\alpha + k)^{-1/2}$ term must be removed, in an analogous manner to that in case (6.1) above, using the technique presented by Bleistein [21]. The far-field may then be evaluated in terms of a uniformly-valid asymptotic expansion and an integral of a form which can be written in terms of Weber functions. Qualitatively, local analysis both near and away from the branch cut show that near the critical angles $\theta = \pm\cos^{-1}k/K$ the diffracted wave field is of order $(kr)^{-1/4}$ and away from those angles the diffracted wave field is of order $(kr)^{-1/2}$. However, cancellation between the contributions from the two distinct integration contours guarantees that the overall diffracted wave field is again order $(kr)^{-1/2}$. This behaviour may be recovered from the asymptotic form of the solution found using Bleistein's method.

In each of these special cases the resulting radiated field is $O(kr^{-1/2})$ and the analysis above is required only to determine the directivity coefficients at various observation angles.

7. Numerical results

7.1. Compressional and shear body waves

As shown above, the motion of a vibrating finite-strip transducer generates cylindrical body waves radiating from the corners at $x = l$ and $-l$. Using the symmetry we may write

$$\begin{aligned}\phi(r,\theta) &= \phi^{(0)}(r,\theta) + \varepsilon^3\phi_l^{(3)}(r,\theta) + \varepsilon^3\phi_{-l}^{(3)}(r,\theta) + O(\varepsilon^2) + O(kr^{-3/2})\\ &\sim D^{(0)}(\theta)\frac{\mathrm{e}^{\mathrm{i}kr}}{\sqrt{kr}} + \varepsilon^3 D^{(3)}(\theta)\frac{\mathrm{e}^{\mathrm{i}kr}}{\sqrt{kr}}.\end{aligned} \tag{87}$$

The leading order solution here is uniformly $O(\varepsilon^0)$, whereas the first correction term is $O(\varepsilon^3)$, except within an angular distance $O(\varepsilon)$ of the critical angles ($\theta = 0, \pi$) where it is $O(\varepsilon^2)$, due to the fact that $D^{(3)}$ jumps order and becomes order $O(\varepsilon^{-1})$. The discarded terms are $O(\varepsilon^4)$, except near the critical angles where again these change

order to $O(\varepsilon^3)$. The compressional wave diffraction coefficient $D^{(3)}(\theta)$ is given by

$$D^{(3)}(\theta) = k\sin\theta \frac{\mathrm{e}^{-\mathrm{i}\pi/4}}{\sqrt{2\pi}} \frac{(\mathrm{i}k\cos\theta, \quad \delta(-k\cos\theta))}{k^2\cos^2\theta - \gamma(k\cos\theta)\delta(k\cos\theta)} \mathbf{U}_+^{(3)}(-k\cos\theta) \tag{88}$$

and $\mathbf{U}_+^{(3)}$ is as given in Eq. (48). Similarly, we may write

$$\begin{aligned}\psi(r,\theta) &= \psi^{(0)}(r,\theta) + \varepsilon^3\psi_l^{(3)}(r,\theta) + \varepsilon^3\psi_{-l}^{(3)}(r,\theta) + O(\varepsilon^2) + O(kr^{-3/2}) \\ &\sim \tilde{D}^{(0)}(\theta)\frac{\mathrm{e}^{\mathrm{i}kr}}{\sqrt{kr}} + \varepsilon^3\tilde{D}^{(3)}(\theta)\frac{e^{\mathrm{i}Kr}}{\sqrt{Kr}},\end{aligned} \tag{89}$$

where the shear wave diffraction coefficient, $\tilde{D}^{(3)}$ is given by

$$\tilde{D}^{(3)}(\theta) = K\sin\theta \frac{\mathrm{e}^{-\mathrm{i}\pi/4}}{\sqrt{2\pi}} \frac{(\gamma(-K\cos\theta), \ -\mathrm{i}K\cos\theta)}{K^2\cos^2\theta - \gamma(K\cos\theta)\delta(K\cos\theta)} \mathbf{U}_+^{(3)}(-K\cos\theta), \tag{90}$$

and this is $O(\varepsilon^0)$ except near the critical angles $\theta = \arccos k/K$ and $\theta = \pi - \arccos k/K$, where it is $O(\varepsilon^{-2})$. The magnitude of the functions $D^{(3)}$ and $\tilde{D}^{(3)}$ are shown in Fig. 5.

The compressional wave diffraction coefficient, $D^{(3)}$ obtains its maximum value near $\theta = 0, \pi$ (see Fig. 5). In the far-field, however, Fig. 6 reveals that the compressional wave potential is dominated by the contribution from the Fresnel terms, and the correction terms are small enough that they may be neglected everywhere. Noting that the ratio $\sin(kl\sin\xi)/k\sin\frac{1}{2}\xi$ has a maximum value of $2l$, it can be seen from the asymptotic form given in Eq. (71) the maximum value for the diffraction coefficient behaves, for large l, like $l\sqrt{2/\pi}$, and thus as the length of the transducer increases, the compressional wave energy is increasingly focused in the direction perpendicular to the surface.

Turning to the shear wave diffraction coefficient, $\tilde{D}^{(3)}$, it transpires that it has sharp peaks near the critical values $\theta = \cos^{-1}k/K, \pi - \cos^{-1}k/K$, where the steepest descent contour is close to the branch cut at $\alpha = \pm k$. When the correction term, $\varepsilon^3\tilde{D}^{(3)}$, is combined with the first approximation, $\tilde{D}^{(0)}$, as shown Fig. 7, only these peaks distinguish the corrected wave-field from the uncorrected wave-field.

7.2. The excited Rayleigh surface wave

As well as the body waves described above, the transducer also induces outgoing Rayleigh surface waves. The magnitude of the excited wave may be determined by considering the contribution from the poles at k_0 (for the left-going wave) and $-k_0$ (for the right-going wave). Because of the symmetry we need consider only the right-going wave, which exists in the region $x > l$. Writing the first approximation to this Rayleigh wave

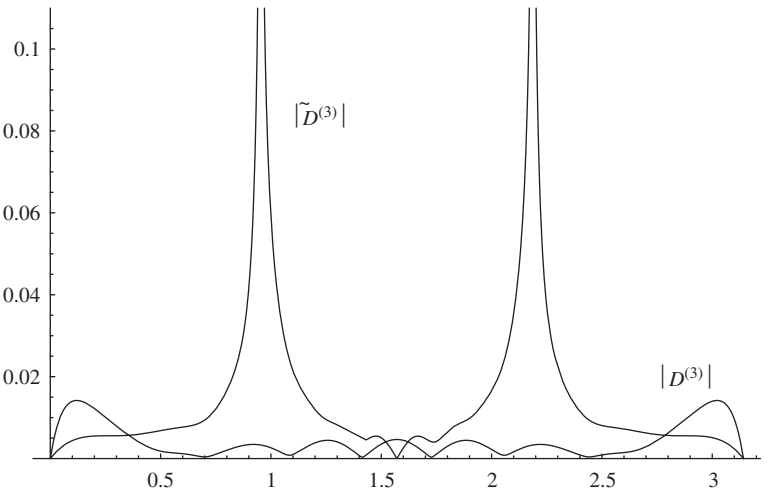

Fig. 5. The first corrections, $|D^{(3)}(\theta)|$ and $|\tilde{D}^{(3)}(\theta)|$, to the compressional and shear diffraction coefficients for a rigid transducer.

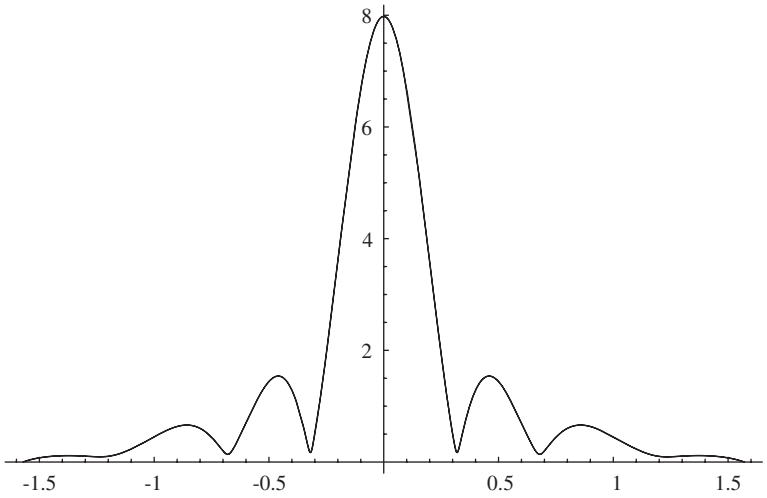

Fig. 6. The corrected and uncorrected compressional diffraction coefficients, $|D^{(0)} + D^{(3)}|$ and $|D^{(0)}|$ as a function of the polar angle ξ. The correction term is small enough for the graphs to be indistinguishable.

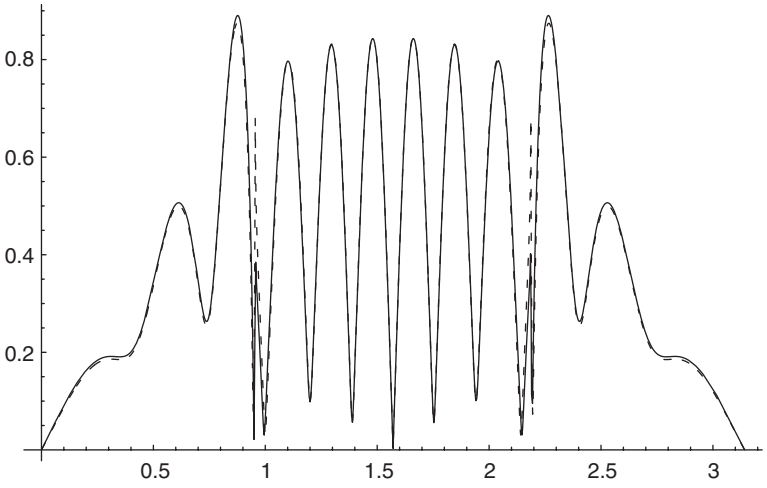

Fig. 7. The corrected (dashed line) and uncorrected (solid line) shear diffraction coefficients, $|\tilde{D}^{(0)} + \tilde{D}^{(3)}|$ and $|\tilde{D}^{(0)}|$ for the rigid transducer, $kl = 10$, $\nu = .25$.

term as

$$\phi_R^{(0)} = C_R^{(0)} \mathrm{e}^{\mathrm{i}k_0(x-l)-\gamma_0 y}, \tag{91}$$

we obtain

$$C_R^{(0)} = \frac{(K^2 - 2k_0^2, \quad 2\mathrm{i}k_0\delta_0)}{R_0 k_0} \mathbf{K}_-^{-1}(-k_0)\mathbf{K}_+^{-1}(0)\begin{pmatrix} 0 \\ 1 \end{pmatrix}, \tag{92}$$

where $\gamma_0 = \gamma(k_0)$ and $\delta_0 = \delta(k_0)$. Similarly, we may show the first correction to the Rayleigh wave coefficient to be

$$\phi_R^{(3)} = \frac{\varepsilon^3}{2\pi\mathrm{i}R_0}(2k_0^2 - K^2, -2\mathrm{i}k_0\delta_0)\mathbf{K}_-^{-1}(-k_0) \times \left\{ \frac{1}{k} F\left(\frac{k-k_0}{k}\right)\mathbf{P}_0\mathbf{K}_+(k) + \frac{1}{K} F\left(\frac{K-k_0}{k}\right)\mathbf{P}_1\mathbf{K}_+(K) \right\} \mathbf{K}_+^{-1}(0)\begin{pmatrix} 0 \\ 1 \end{pmatrix}. \tag{93}$$

The radiated Rayleigh wave coefficient, $|C_R|$ is plotted in Figs. 8 and 9 at leading order (dashed) and with first correction (solid). The first figure indicates that edge interference effects alter the Rayleigh wave coefficient from its constant value, and in the latter figure kl is fixed at 10 and Poisson's ratio v is varied. The surface wave amplitude decreases monotonically with Poisson's ratio, and here we see that the correction term has little effect on the overall trend.

7.3. Balance of energy per unit cycle

In order to obtain a check on the accuracy of the various approximations used in the solution of the problem of a forced transducer, it is useful to perform an energy balance calculation. It is possible to obtain expressions for the work done per unit cycle by the motion of the transducer against the stress field at the surface and the energy radiated at a large distance by the excited waves. Since there are no sources of energy

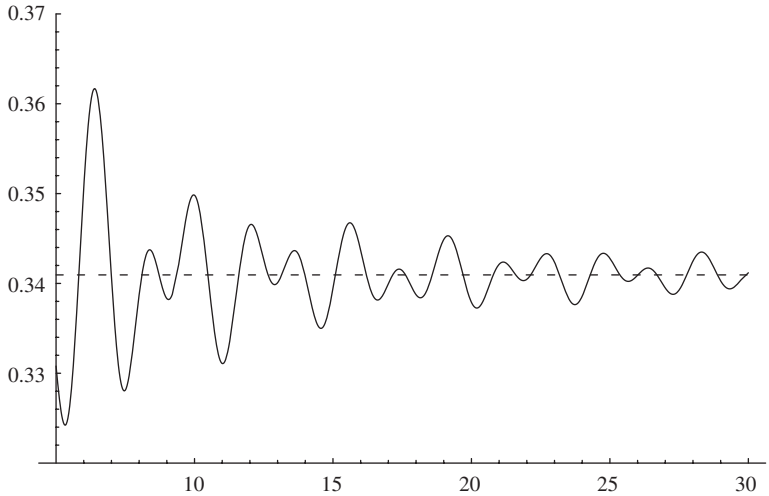

Fig. 8. Coefficient of the Rayleigh surface wave excited by the rigid transducer for the case $v = .25$ and varying values of kl. The dashed line is for an infinite transducer (leading order solution) and the solid line includes the first correction term.

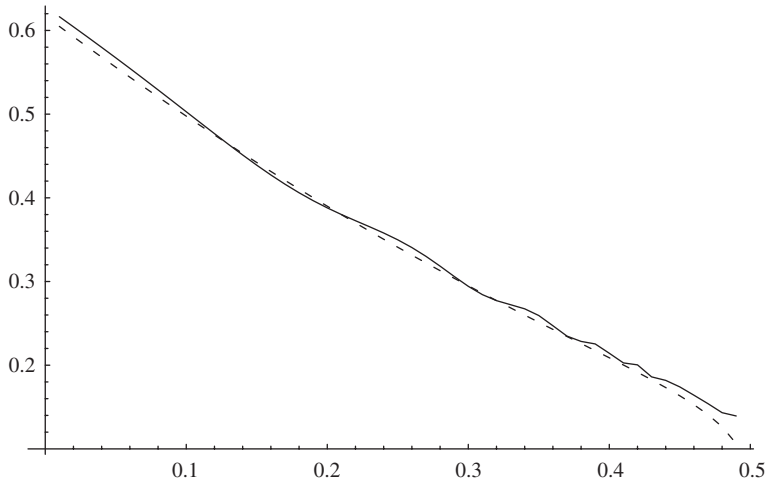

Fig. 9. Coefficient of the Rayleigh surface wave excited by the rigid transducer for the case $kl = 10$ and varying values of Poisson's ratio v. The dashed line is for an infinite transducer (leading order solution) and the solid line includes the first correction term.

within the half-space, these physical quantities must be equal, and the degree by which they differ in our approximate solution is indicative of the accuracy of that solution.

By integrating over a semi-circular contour of large radius (see Fig. 10) it can be shown (see Ref. [22]) that the energy radiated in a single period by outgoing compressional and shear waves of the form

$$\phi \sim \frac{D_c(\theta)}{\sqrt{kr}} e^{ikr}, \quad \psi \sim \frac{D_s(\theta)}{\sqrt{Kr}} e^{iKr}, \tag{94}$$

is given by

$$E_C = \pi\mu K^2 \int_0^\pi |D_c(\theta)|^2 \, d\theta \quad \text{and} \quad E_S = \pi\mu K^2 \int_0^\pi |D_s(\theta)|^2 \, d\theta, \tag{95}$$

respectively. Similarly, the energy radiated in a Rayleigh surface wave of amplitude A_R is given by

$$E_R = \pi\mu K^2 |A_R|^2 \left\{ \frac{k_0(\delta_0^2 + \gamma_0^2)}{2\gamma_0\delta_0^2} - \frac{4k_0^4 - K^4}{4k_0^3\delta_0} \right\}. \tag{96}$$

It can also be shown that the work done by the transducer over one period is given by

$$\pi \operatorname{Im}\left\{ \int_{-l}^{l} \overline{u}_i \sigma_{ij} \nu_j \, ds \right\} = 0, \tag{97}$$

where $\mathbf{u}$ and σ_{ij} are the complex-valued velocity field and stress tensor. For the rigid transducer modelled in Section 2 and solved in Section 5, the integrand in Eq. (97) vanishes on the free surface, for all $x \notin [-l, l]$. Hence, for the unit forcing given in Eq. (40), it is clear from the definition in Eq. (20) that the integral is given by

$$\pi \operatorname{Im}(\Sigma_{22}^1(0)) = -\mu\pi K^2 \operatorname{Im}(\Phi(0,0)). \tag{98}$$

The first approximation to $\Phi(\alpha, 0)$ is given by

$$\Phi^{(0)}(\alpha, 0) = \frac{(i\alpha, \quad -\delta)}{i\alpha(\alpha^2 - \gamma\delta)} \left\{ e^{i\alpha l} \mathbf{K}_+(\alpha) - e^{-i\alpha l} \begin{pmatrix} -1 & 0 \\ 0 & 1 \end{pmatrix} \mathbf{K}_+(-\alpha) \right\} \mathbf{K}_+^{-1}(0) \begin{pmatrix} 0 \\ 1 \end{pmatrix}, \tag{99}$$

expanding the analytic terms in Eq. (99) as Taylor series about $\alpha = 0$ and formally taking the limit as $\alpha \to 0$ gives

$$\Phi^{(0)}(0,0) = \frac{2li}{k} + (0, \quad 2/k)\mathbf{K}_+'(0)\mathbf{K}_+^{-1}(0) \begin{pmatrix} 0 \\ 1 \end{pmatrix}, \tag{100}$$

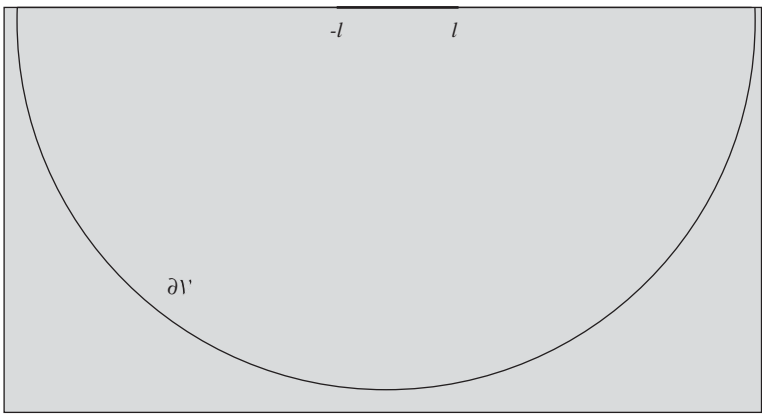

Fig. 10. Semi-circular closed loop $\partial\mathcal{V}$.

where $\mathbf{K}'_+(\alpha)$ denotes $(\mathrm{d}/\mathrm{d}\alpha)\mathbf{K}_+(\alpha)$. Recalling the Khrapkov–Daniele form of the Wiener–Hopf factor $\mathbf{L}_+$, given in Eq. (26), and that $\mathbf{K}_+ = \mathbf{L}_+\mathbf{M}$, we can easily show

$$\mathbf{K}_+^{-1}(0) = r_+^{-1}(0)\mathbf{M}^{-1}(0) \tag{101}$$

and can explicitly differentiate $\mathbf{K}_+$ to obtain

$$\mathbf{K}'_+(0) = r'_+(0)\mathbf{M}(0) - r_+(0)s'_+(0)\mathbf{J}(0)\mathbf{M}(0) + r_+(0)\mathbf{M}'(0), \tag{102}$$

where we have employed $\mathbf{J}'(0) = \mathbf{0}$ since $\mathbf{J}$ is even in α. Differentiating the integral form of $r_+(\alpha)$ found in Eq. (29) gives

$$r'_+(0) = \left(\frac{-1}{2k_0} + g(0)\right) r_+(0), \tag{103}$$

where $g(\alpha)$ is given by

$$g(\alpha) = \frac{1}{4\pi\mathrm{i}} \int_{-K}^{-k} \log\left[\frac{S(\xi)(\xi^2 - \gamma\delta)}{R(\xi)(\xi^2 + \gamma\delta)}\right] \frac{\mathrm{d}\xi}{(\xi - \alpha)^2}. \tag{104}$$

In the interval $[-K, -k]$, $|S(\xi)| = |R(\xi)|$ and $|\xi^2 - \gamma\delta| = |\xi^2 + \gamma\delta|$. Thus the integral in Eq. (104) is pure imaginary, hence $g(\alpha)$ is real, and so $r'_+(0)$ has the same argument as $r_+(0)$. Differentiating the Wiener–Hopf sum decomposition for $s_\pm$ from Eq. (27), and substituting from Eq. (30), gives

$$\begin{aligned} s'_+(0) + s'_-(0) &= 2s'_+(0) \\ &= \frac{\mathrm{d}}{\mathrm{d}\alpha} \tan^{-1}\left\{\frac{-\mathrm{i}\alpha(2\alpha^2 - K^2 - 2\gamma\delta)}{K^2\sqrt{\gamma\delta}}\right\}\Bigg|_{\alpha=0} = \frac{2kK - K^2}{K^2\sqrt{kK}}. \end{aligned} \tag{105}$$

Hence $s'_+(0)$ is also real. Finally, the singularities and zeros of the Padé approximant f_N all lie on the real line. Therefore, the coefficients in the meromorphic matrix $\mathbf{M}$ given in Eq. (34) are also real. This means that $\mathbf{M}(0)$ must be real; the same is true for $\mathbf{J}(0)$. It can now be seen that all the elements of the matrix $\mathbf{K}'_+(0)$ have the same argument as $r_+(0)$, and hence all the elements of $\mathbf{K}'_+(0)\mathbf{K}_+^{-1}(0)$ are real. Therefore, the second term in Eq. (100) does not contribute to the work done by the transducer, yielding

$$\mathrm{Im}(\Phi^{(0)}(0,0)) = \frac{2l}{k}. \tag{106}$$

The evaluation of $\Phi^{(3)}(0,0)$ is more straightforward and it can be seen from Eq. (51) that

$$\mathrm{Im}(\Phi^{(3)}(0,0)) = (0,\ \ 1/k)\mathrm{Re}\{\mathbf{U}_+^{(3)}(0) + \mathbf{U}_-^{(3)}(0)\}. \tag{107}$$

We can now determine the work done, which is shown in Fig. 11 over a range of kl. It transpires that, even for moderate values of kl the first correction term does not make any significant contribution to the total work done.

As can be seen from the numerical results presented in Tables 1 and 2 the error terms both with and without the first correction term are of order ε^6 ($\varepsilon = 10^{-1/2}$ for the given value of kl), which is consistent with the largest neglected term being order ε^4 and the total work by the transducer being of order ε^{-2}. Although the addition of the correction term to the solution does not improve the order of magnitude of the discrepancy in the energy, it does provide an estimate of known accuracy for the multiply diffracted wavefield, as well as capturing its key features.

8. Concluding remarks

This paper has outlined a procedure for determining the elastic field radiating from a two-dimensional flat plate transducer into an elastic half-space. The major difficulty encountered in the analysis, namely the factorization of the matrix Wiener–Hopf kernel, is due to the physical complexity of having mixed boundary conditions on the faces of the elastic body. The Wiener–Hopf approximant matrix technique enables a fast and accurate approximate factorization of a Wiener–Hopf kernel for which no exact factorization is known.

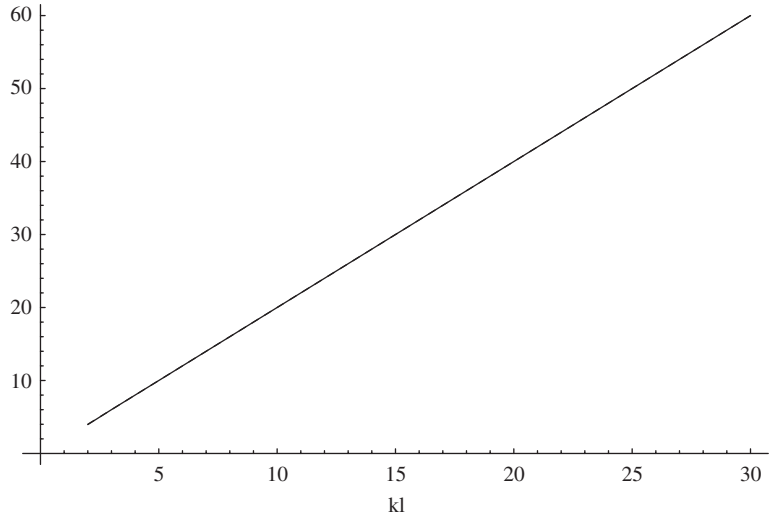

Fig. 11. The non-dimensionalised work done by the rigid transducer, $\mathrm{Im}\{\Phi^{(0)}(0,0)+\Phi^{(3)}(0,0)\}$ and $\mathrm{Im}\{\Phi^{(0)}(0,0)\}$. The corrected value cannot be distinguished from the first approximation. ($v = .25$).

Table 1
Non-dimensionalised energy partition for the leading order approximation to the solution for the finite rigid transducer

v	Energy in	Energy out				% error
	Total	E_C/μ	E_S/μ	E_R/μ	Total/μ	
0.1	141.372	133.345	5.402	2.584	141.331	0.03
0.25	188.495	179.039	6.551	2.719	188.309	0.10
0.4	376.991	360.322	12.591	3.711	376.624	0.09

Table 2
Non-dimensionalised energy partition including the first correction term for the finite rigid transducer, $kl = 10$

v	Energy in	Energy out				% error
	Total	E_C/μ	E_S/μ	E_R/μ	Total/μ	
0.1	141.379	133.288	5.353	2.638	141.279	0.07
0.25	188.511	178.923	6.471	2.862	188.257	0.13
0.4	377.060	359.641	12.689	3.905	376.235	0.22

The method appears to give good accuracies even for modest Padé number and for transducers of lengths larger than just a few wavelengths. The method of solution herein is designed to be adaptable to more complicated one-dimensional models of the transducer, such as impedance surfaces or ones in which the electric and elastic fields are coupled. The advantage of the present approach over direct numerical schemes is that the essential analytical properties of the solution are not lost in the approximation procedure, and so gross features and trends over parameter ranges are clearly discernible. The latter property is extremely useful for the design of transducers to be used for non-destructive evaluative purposes.

The solutions of the diffraction problem considered is derived by exploiting the symmetry of the geometry and forcing. These symmetric configurations were chosen for convenience and cases which are fully asymmetric may also be analysed using similar methods. In asymmetric problems the modified matrix

Wiener–Hopf technique results in a pair of coupled vector Fredholm integrations of the form:

$$\mathbf{\Psi}_+(\alpha) = \mathbf{f}_1(\alpha) + \int \boldsymbol{\kappa}_1(\xi,\alpha)\mathbf{\Psi}_-(\xi)\,\mathrm{d}\xi, \tag{108}$$

$$\mathbf{\Psi}_-(\alpha) = \mathbf{f}_2(\alpha) + \int \boldsymbol{\kappa}_2(\xi,\alpha)\mathbf{\Psi}_+(\xi)\,\mathrm{d}\xi. \tag{109}$$

These may be iterated by substituting the leading order solution for $\mathbf{\Psi}_+(\alpha)$ from Eq. (108) into Eq. (109) and vice versa.

The Wiener–Hopf approximant matrix technique lends itself to a wider variety of boundary value problems than considered here. In formulating Wiener–Hopf functional equations from boundary value problems the physics of the problem and the nature of the boundary conditions are contained within the singularity structure of the Wiener–Hopf kernel. For example, some non-destructive evaluation techniques, such as the acoustic microscope, immerse the specimen in fluid and insonify it using acoustic waves. The dispersion relation for such a problem admits a propagating interfacial wave (the Schölte wave) as well as a leaky Rayleigh wave. Application of the Wiener–Hopf approximant matrix technique to a Wiener–Hopf kernel associated with such a boundary value problem would allow for quantitative predictions to be made about the excitation of these waves.

Appendix A. Approximation of the branch-cut integrals

The integrals in Eq. (43) may be approximated by the use of Watson's Lemma. Making a routine change of variables,

$$\int_{\mathscr{C}_k} \mathrm{e}^{-2\mathrm{i}\xi l}\mathbf{K}_+^{-1}(\xi)\mathbf{f}(\xi)\frac{\mathrm{d}\xi}{\xi-\alpha} = \mathrm{i}k\mathrm{e}^{2\mathrm{i}kl}\int_0^\infty \mathrm{e}^{-2z/\varepsilon^2}\Delta_k\mathbf{f}(-k-\mathrm{i}kz)\frac{\mathrm{d}z}{\alpha+k+\mathrm{i}kz} \tag{A.1}$$

and

$$\int_{\mathscr{C}_K} \mathrm{e}^{-2\mathrm{i}\xi l}\mathbf{K}_+^{-1}(\xi)\mathbf{f}(\xi)\frac{\mathrm{d}\xi}{\xi-\alpha} = \mathrm{i}k\mathrm{e}^{2\mathrm{i}Kl}\int_0^\infty \mathrm{e}^{-2z/\varepsilon^2}\Delta_K\mathbf{f}(-K-\mathrm{i}kz)\frac{\mathrm{d}z}{\alpha+K+\mathrm{i}kz}, \tag{A.2}$$

where Δ_K and Δ_k denote the jump in $\mathbf{K}_+^{-1}$ from the left to the right side of the cuts vertically downwards from $-K$ and $-k$ respectively.

The dominant contribution to each of these integrals comes from a neighbourhood of $z=0$, and we can expand the integrand as a Taylor series about this point (i.e. around $-k$ or $-K$ as appropriate). We can write the first coefficient in this series explicitly in terms of $\mathbf{K}_-(-k)$ and numerically calculate as many of the remaining coefficients as required, by repeated differentiation of Eqs. (29) and (30) and substitution into Eq. (26). We shall consider only the lowest order term.

Explicitly calculating the Taylor series for the elements of $\mathbf{K}^{-1}$, given in Eq. (24), gives

$$\Delta_k(-k-\mathrm{i}kz) = \mathbf{K}_-(-k)\mathbf{K}_0 z^{1/2} + O(z^{3/2}), \tag{A.3}$$

$$\Delta_K(-K-\mathrm{i}kz) = \mathbf{K}_-(-K)\mathbf{K}_1 z^{1/2} + O(z^{3/2}), \tag{A.4}$$

where

$$\mathbf{K}_0 = 2^{3/2}\frac{K^2\mathrm{e}^{\mathrm{i}\pi/4}}{k^3}\begin{pmatrix} \mathrm{i}k\delta(k) & k^2-K^2 \\ -k^2 & \mathrm{i}k\delta(k)\end{pmatrix} \tag{A.5}$$

and

$$\mathbf{K}_1 = 2^{3/2}\frac{\mathrm{e}^{-3\mathrm{i}\pi/4}\sqrt{kK}}{K^2}\begin{pmatrix} -\mathrm{i}K\gamma(K) & -K^2 \\ K^2-k^2 & -\mathrm{i}K\gamma(K)\end{pmatrix}. \tag{A.6}$$

Hence, we may evaluate the integrals in terms of a series in increasing powers of ε. For $\alpha \in \mathscr{D}$.

$$\int_0^\infty \mathrm{e}^{-2z/\varepsilon^2} \Delta_k \mathbf{f}(-k - \mathrm{i}kz) \frac{\mathrm{d}z}{\alpha + k + \mathrm{i}kz} = \mathbf{K}_-(-k)\mathbf{K}_0\mathbf{f}(-k) \int_0^\infty \mathrm{e}^{-2z/\varepsilon^2} \frac{z^{1/2}\mathrm{d}z}{\alpha + k + \mathrm{i}kz} + O(\varepsilon^5), \tag{A.7}$$

and the integral in (A.7) may be rewritten as a special function:

$$\int_0^\infty \mathrm{e}^{-2z/\varepsilon^2} \sqrt{z} \frac{\mathrm{d}z}{\alpha + k + \mathrm{i}kz} = \frac{\varepsilon^3}{2^{3/2}} \int_0^\infty \sqrt{p}\mathrm{e}^{-p} \frac{\mathrm{d}p}{\alpha + k + \mathrm{i}k\varepsilon^2 p/2} = \frac{\varepsilon^3}{\mathrm{i}k\sqrt{2}} \left[\frac{1}{\varepsilon^2} W_0\left(-\frac{2\mathrm{i}}{\varepsilon^2} \left(\frac{\alpha + k}{k} \right) \right) \right], \tag{A.8}$$

where $2W_0(z) = \sqrt{\pi}\mathrm{e}^{z/2} z^{-1/4} W_{-\frac{3}{4},\frac{1}{4}}(z)$ and $W_{k,m}(z)$ is a Whittaker function (see Abramowitz and Stegun [23, Section 13.2]). If we define $F(z)$ by

$$F(z) = \frac{1}{\varepsilon^2} W_0\left(-\frac{2\mathrm{i}z}{\varepsilon^2} \right), \tag{A.9}$$

then, from the asymptotic form of $W_{k,m}$, it can be seen that if z is $O(1)$, then $F(z)$ is no larger than $O(\varepsilon^0)$. Expressions for the other branch cut integrals and for higher order terms in the asymptotic series may be derived in exactly the same manner. Thus,

$$\int_{\mathscr{C}_k} \mathrm{e}^{-2\mathrm{i}\xi l} \mathbf{K}_+^{-1}(\xi)\mathbf{f}(\xi) \frac{\mathrm{d}\xi}{\xi - \alpha} \sim \varepsilon^3 \mathbf{P}_0 \mathbf{f}(-k) F\left(\frac{\alpha + k}{k} \right) \tag{A.10}$$

and

$$\int_{\mathscr{C}_K} \mathrm{e}^{-2\mathrm{i}\xi l} \mathbf{K}_+^{-1}(\xi)\mathbf{f}(\xi) \frac{\mathrm{d}\xi}{\xi - \alpha} \sim \varepsilon^3 \mathbf{P}_1 \mathbf{f}(-K) F\left(\frac{\alpha + K}{k} \right), \tag{A.11}$$

where

$$\mathbf{P}_0 = \frac{\mathrm{e}^{2\mathrm{i}kl}}{\sqrt{2}} \mathbf{K}_-(-k)\mathbf{K}_0 \quad \text{and} \quad \mathbf{P}_1 = \frac{\mathrm{e}^{2\mathrm{i}Kl}}{\sqrt{2}} \mathbf{K}_-(-K)\mathbf{K}_1. \tag{A.12}$$

In $\mathscr{D}$, the domain in which we wish to solve the integral equation, $F((\alpha + k)/k)$ and $F((\alpha + K)/k)$ are $O(1)$ quantities.

References

[1] P.H. Rogers, Mathematical model for a free-flooded piezoelectric cylinder transducer, *Journal of Acoustic Society of America* 80 (1986) 13–18.

[2] E.R. Lapwood, The disturbance due to a line source in a semi-infinite elastic medium, *Philosophical Transactions of the Royal Society of London A* 242 (1949) 63–100.

[3] G.R. Wickham, The forced two-dimensional oscillations of a rigid strip in smooth contact with a semi-infinite elastic solid, *Mathematical Proceedings of the Cambridge Philosophical Society* 81 (1976) 291–311.

[4] G.R. Wickham, Short-wave radiation from a rigid strip in smooth contact with a semi-infinite elastic solid, *Quaterly Journal of Mechanics and Applied Mathematics* 33 (1980) 409–429.

[5] J.D. Achenbach, A.K. Gautesen, H. McMaken, *Ray Methods for Waves in Elastic Solids with Applications to Scattering by Cracks*, Pitman, Boston, 1982.

[6] L.M. Flitman, On the motion of a rigid strip-mass lying on an elastic half space and excited by a seismic wave, *Journal of Applied Mathematics and Mechanics* 26 (1962) 1582–1604.

[7] M.A. Oien, Steady motion of a rigid strip bonded to an elastic half space, *Journal of Applied Mechanics* 38 (1971) 328–344.

[8] C.A. Brebbia, S. Walker, *Boundary Element Techniques in Engineering*, Newnes-Butterworths, London, 1980.

[9] D.E. Beskos, Boundary element methods in dynamic analysis, *Applied Mechanics Review* 40 (1987) 1–23.

[10] D. Gridin, L.J. Fradkin, The high-frequency asymptotic description of pulses radiated by a circular normal transducer into an elastic half-space, *Journal of Acoustic Society of America* 104 (1998) 3190–3198.

[11] B. Noble, *Methods Based on the Wiener–Hopf Technique*, second ed., Chelsea, New York, 1988.

[12] I.D. Abrahams, Radiation and scattering of waves on an elastic half-space: a non-commutative matrix Wiener–Hopf problem, *Journal of Mechanics and Physics of Solids* 44 (1996) 2125–2154.
[13] I.D. Abrahams, On the solution of Wiener–Hopf problems involving non-commutative matrix kernel decompositions, *SIAM Journal of Applied Mathematics* 57 (1997) 541–567.
[14] P.J. Gould, *Introduction to Linear Elasticity*, second ed., Springer, Berlin, 1994.
[15] D.S. Jones, Diffraction by a wave guide of finite length, *Proceedings of the Cambridge Philosophical Society* 48 (1952) 118–134.
[16] D.G. Crighton, A.P. Dowling, J.E. Ffowcs Williams, M. Heckl, F.G. Leppington, *Modern Methods in Analytical Acoustics*, Springer, Berlin, 1992.
[17] A.A. Khrapkov, Certain cases of the elastic equilibrium of an infinite wedge with a non-symmetric notch at the vertex subject to concentrated forces, *Applied Mathematics and Mechanics (PMM)* 35 (1971) 625–637.
[18] V.G. Daniele, On the factorization of Wiener–Hopf matrices in problems solvable with Hurd's method, *IEEE Transactions on Antennas and Propagation* AP-26 (1978) 614–616.
[19] G.A. Baker, P. Graves-Morris, *Padé Approximants*, second ed., Cambridge University Press, Cambridge, 1996.
[20] I.D. Abrahams, The application of Padé approximants to Wiener–Hopf factorization, *IMA Journal of Applied Mathematics* 65 (2000) 257–281.
[21] N. Bleistein, Uniform asymptotic expansions of integrals with stationary point near algebraic singularity, *Common and Pure Applied Mathematics* 19 (1966) 353–370.
[22] F.L. Neerhoff, Reciprocity and Power-Flow Theorems for Scattering of Plane Elastic Waves in a Half-space, *Wave Motion* 2 (1980) 99–113.
[23] M. Abramowitz, I.A. Stegun, *Handbook of Mathematical Functions*, Dover Publications, New York, 1965.